NASA TECHNICAL REPORT

NASA TR R-311

c. 1

NASA TR R-311

INVISCID RADIATING SHOCK LAYERS ABOUT SPHERES TRAVELING AT HYPERBOLIC SPEEDS IN AIR

by Richard W. Barnwell

Langley Research Center
Langley Station, Hampton, Va.

NATIONAL AERONAUTICS AND SPACE ADMINISTRATION • WASHINGTON, D. C. • MAY 1969

Completed 20 Oct 70 Jw

ERRATA

NASA Technical Report R-311

INVISCID RADIATING SHOCK LAYERS ABOUT SPHERES TRAVELING AT HYPERBOLIC SPEEDS IN AIR

By Richard W. Barnwell

May 1969

Page 55, equation (B3): This equation, which is part of the curve fit for the thermodynamic properties of equilibrium air, contains two erroneous numbers. The correct form of the equation is

The results presented in the report are consistent with the correct equation.

Page 67, figure 24: The exact solution shown in the figure is given by equation (43) rather than equation (46) as indicated.

NASA-Langley, 1970

Issued 10-13-70

INVISCID RADIATING SHOCK LAYERS ABOUT SPHERES TRAVELING AT HYPERBOLIC SPEEDS IN AIR

By Richard W. Barnwell

Langley Research Center
Langley Station, Hampton, Va.

NATIONAL AERONAUTICS AND SPACE ADMINISTRATION

For sale by the Clearinghouse for Federal Scientific and Technical Information
Springfield, Virginia 22151 – CFSTI price $3.00

INVISCID RADIATING SHOCK LAYERS ABOUT SPHERES TRAVELING AT HYPERBOLIC SPEEDS IN AIR*

By Richard W. Barnwell
Langley Research Center

SUMMARY

Time-dependent finite-difference techniques are used to obtain numerical solutions for the problem of the inviscid flow of radiating equilibrium air past spheres traveling at hyperbolic speeds. The effects of absorption are included, and results are presented for both gray and nongray absorption coefficient models for spheres with different radii. It is shown that the nondimensional heat-flux distributions for the gray and nongray models are similar and that these distributions are weak functions of the radius of the sphere and the altitude and strong functions of the flight velocity.

INTRODUCTION

The problem of radiating flow past blunt bodies traveling at hyperbolic speeds in air has been the subject of intensive theoretical investigation during the past decade. Solutions have been obtained for inviscid and viscous flows and for both transparent and absorbing radiation models. In reference 1, Goulard has investigated transparent, inviscid flow fields. Thomas (ref. 2) has extended Goulard's work to include the effects of absorption for cases for which the absorption coefficient is small by replacing the absorption integral at a point in the flow field with a Taylor series expansion about the point. An iterative numerical procedure is used by Howe and Viegas (ref. 3) to treat viscous flow fields which emit and absorb thermal radiation. Olstad (refs. 4 and 5) employs the Poincaré-Lighthill-Kuo method to obtain perturbation solutions to the inviscid radiation problem. Callis (ref. 6) solves this same problem with a time-dependent finite-difference technique of second-order accuracy. In all the references cited, modified one-dimensional flow fields are considered, and the solutions which are obtained are applicable in the vicinity of the stagnation streamline.

---

*An earlier version of part of the analysis which is presented in this paper was used as a thesis in partial fulfillment of the requirements for the degree of Doctor of Philosophy in Engineering Mechanics, Virginia Polytechnic Institute, Blacksburg, Virginia, June 1968.

Solutions which are not restricted to the stagnation streamline are presented in references 7 to 10. In references 7 and 8, Hoshizaki and Wilson use an integral method to obtain solutions for inviscid and viscous flows, respectively, for a transparent radiation model. These authors extend their work to include the effects of absorption in reference 9. Cheng and Vincenti (ref. 10) use an inverse method to treat the problem of inviscid flow past blunt bodies and consider the effects of absorption.

The frequency dependence of the absorption coefficient for high-temperature air is considered in references 4, 5, 6, 9, and 11. Hoshizaki and Wilson (ref. 9) perform the integration with respect to frequency in the radiative heat-transfer term of the energy equation numerically, whereas Olstad (refs. 4 and 5) and Smith and Hassan (ref. 11) use step functions to approximate the frequency-dependent absorption coefficient and perform the integration with respect to frequency analytically. The step-function absorption coefficient models are constructed by dividing the spectrum into intervals and using mean values of the absorption coefficients for each interval.

In the present paper, the computation of the radiating shock layer about a sphere is made by using a time-dependent method of first-order accuracy. This method is a "discrete shock" method which is similar to that of Moretti and Abbett (ref. 12). The shock wave is treated as a boundary at which the flow properties are discontinuous. With time-dependent, finite-difference methods, one can avoid the assumption of functional forms for some of the normal flow property profiles as is done with the integral method which is used in references 7, 8, and 9. Another advantage is that time-dependent methods can be used to solve the direct blunt-body radiation problem as opposed to the inverse problem, which is solved in reference 10.

The problem of time-dependent supersonic flow about a blunt body is treated as an initial-value problem. By starting with an initial approximate solution, the solution is determined at successive time steps until the steady solution is approached asymptotically. The inclusion of the partial derivatives with respect to time in the equations for fluid flow makes those equations hyperbolic at all points in the flow field including regions where the flow is subsonic. This feature makes the time-dependent approach an attractive one for computing supersonic flow past blunt bodies. The governing partial differential equations are approximated with finite-difference equations which are solved with forward-marching techniques.

The time-dependent approach is particularly applicable to the problem of radiating flow with absorption because it provides a straightforward means of solving the energy equation, which is an integro-differential equation. When determining the solution at a new time step, the known solution at the previous step is used to evaluate the integral term.

As was indicated earlier, the present paper treats the inviscid flow fields about spheres traveling at hyperbolic velocities at high altitudes in the earth's atmosphere. Spheres with several different radii are treated, and both frequency-dependent and frequency-independent absorption coefficient models are used. The frequency-dependent absorption coefficient is approximated with a step-function model which is similar to those used in references 4, 5, 6, and 11. It is assumed that the gas in the free stream neither emits nor absorbs thermal energy and that the body surface neither emits nor reflects. For the purpose of calculating the absorption integral in the energy equation, the radiating shock layer is treated as an infinite slab with the same width as the local-shock-layer thickness. The thermodynamic state of the gas is described by curve fits of previously calculated equilibrium air data.

SYMBOLS

$A_i, B_i, C_i, D_i, E_i, F_i$ quantities defined by equations (10)

$A_N[\bar{r},\bar{s}]$ integral defined by equation (E9)

$A_\nu[\bar{r},\bar{s}]$ optical depth defined by equation (40)

a speed of sound

a_o reference speed of sound, 331.8 m/sec

$\tilde{a}_N, \tilde{b}_N$ exponents expressing power-law variation of absorption coefficient with density and temperature, respectively

B_N frequency integral of Planck function defined by equation (E8)

B_ν Planck function

C constant used in equation (37)

$\tilde{C}$ quantity defined by equation (E26)

c speed of light

$\tilde{d}$ exponent expressing power-law variation of shock-layer thickness with $\cos \Theta$

E	total energy per unit mass
$E_n(z)$	exponential integral defined by equation (39)
e	internal energy per unit mass
$F(z)$	function defined by equation (43)
$F\left(1,1;2+\frac{1}{\tilde{N}};\left[1+\frac{\tilde{C}}{\zeta^{\tilde{N}}}\right]^{-1}\right)$	hypergeometric series defined by equation (E28)
f	scale constant used in equation (E16)
$\tilde{f}$	constant defined by equation (E18)
$\tilde{g}$	exponent expressing power-law variation of Planck function with $hc/k\lambda T$
H	total enthalpy per unit mass
h	static enthalpy per unit mass, also Planck constant
h_η	scale constant for η coordinate
$\bar{h}$	altitude
I_ν	radiation intensity
I_ν^+, I_ν^-	radiation intensity away from body surface and toward it, respectively
K	shock curvature
k	Boltzmann constant
l	spatial position, $r = r_b + (l - 1)\Delta r$ and $Y = (l - 1)\Delta Y$
m	spatial position, $\theta = (m - 1)\Delta\theta$ and $\Theta = (m - 1)\Delta\Theta$
M,N,n	integers
$\tilde{N}$	quantity defined by equation (E25)

p	pressure
p_o	reference pressure, 1.013×10^5 newtons/m^2
Q	total radiative heat input per unit volume and time defined by equation (D15)
Q_N	quantity defined by equation (E5)
Q_ν	monochromatic radiative heat input per unit volume and time defined by equation (D9)
q	total radiative heat flux defined by equation (D8)
q_ν	monochromatic radiative heat flux defined by equation (D3)
R	perpendicular distance from axis of symmetry to a point in flow field, also gas constant for air, 2.870×10^2 joules/kg-^oK
R_o	quantity defined by equation (B7)
$\tilde{R},\tilde{S}$	exponents expressing power-law variation of temperature with pressure and density, respectively
r	radial coordinate
S	entropy
T	temperature
T_o	reference temperature, 273.2^o K
t	time
U,V	velocity components normal and parallel to shock wave, respectively
u,v	velocity components normal and parallel to body surface, respectively
$\overline{V}_\infty$	magnitude of free-stream velocity

W	component of shock velocity normal to body surface defined by equation (14)
x	Cartesian coordinate, also Goulard coordinate
Y	nondimensional coordinate normal to body surface defined by equation (11c)
y	coordinate normal to body surface, also Cartesian coordinate
$\bar{y}$	nondimensional coordinate defined by equation (E7)
z	length along line of propagation of radiation
α,α_ν	absorption coefficient
α_N	mean absorption coefficient for interval $\nu_N \leqq \nu \leqq \nu_{N+1}$
α_P	Planck mean absorption coefficient
β	acute angle between normal to shock wave and free-stream direction
Γ	energy depletion parameter defined by equation (46)
Γ_1	energy depletion parameter defined by equation (E22)
γ	ratio of specific heats
$\tilde{\gamma}$	ratio of static enthalpy to internal energy
$\Delta t,\Delta r,\Delta\theta$	mesh spacings for time t and coordinates r and θ, respectively
$\Delta\tau,\Delta Y,\Delta\Theta$	mesh spacings for time τ and coordinates Y and Θ, respectively
δ	shock-layer thickness along a line normal to body surface defined by equation (12)
δ_A	shock-detachment distance for adiabatic flow
ϵ	acute angle between normals to shock wave and body surface

ζ	quantity defined by equation (E23)
η	coordinate along shock wave
θ,Θ	polar angle
λ	wavelength
μ	quantity defined by equations (9)
ν	frequency
ν_N	discrete frequency
ξ	coordinate normal to shock wave
ρ	density
ρ_o	reference density, 1.292 kg/m^3
σ	Stefan-Boltzmann constant
τ	time
ϕ	angle between direction of propagation of radiation and y-axis
ψ	azimuthal angle
Ω	solid angle

Subscripts:

b	at body surface
$j,\hat{j}$	at base point of bicharacteristic
max	maximum
s	immediately behind shock wave

st at stagnation point

w at body point

∞ in free stream

Superscript:

k number of time steps, $t = k\,\Delta t$ and $\tau = k\,\Delta\tau$

ANALYSIS

The procedures which are used to solve the equations for time-dependent, inviscid flow at points within the shock layer, on the shock wave, and on the body surface are described herein. In addition, discussions of the thermodynamic and absorption coefficient models for high-temperature air are presented, the method for evaluating the integral terms in the energy equation is given, and the calculation of the starting solution is discussed. It should be noted that results for steady flow are obtained after many time steps when the time derivatives, which approach zero asymptotically, are sufficiently small.

Calculations at Points Within Shock Layer

Governing equations.- The natural coordinate system for formulating the problem of axisymmetric flow past a sphere is a spherical polar system with its origin located at the center of the sphere and its axis alined with the direction of flow in the free stream. When written in this coordinate system and in conservation form the governing equations are:

Continuity:

$$\frac{\partial(\rho r)}{\partial t} + \frac{\partial(\rho u r)}{\partial r} + \frac{\partial(\rho v)}{\partial \theta} + \rho u + \rho v \cot\theta = 0 \tag{1}$$

Radial momentum:

$$\frac{\partial(\rho u r)}{\partial t} + \frac{\partial\left[\left(p + \rho u^2\right)r\right]}{\partial r} + \frac{\partial(\rho u v)}{\partial \theta} - \left[p - \rho\left(u^2 - v^2\right)\right] + \rho u v \cot\theta = 0 \tag{2}$$

Tangential momentum:

$$\frac{\partial(\rho v r)}{\partial t} + \frac{\partial(\rho u v r)}{\partial r} + \frac{\partial\left(p + \rho v^2\right)}{\partial \theta} + 2\rho u v + \rho v^2 \cot\theta = 0 \tag{3}$$

Energy:

$$\frac{\partial(\rho Er)}{\partial t} + \frac{\partial(\rho uHr)}{\partial r} + \frac{\partial(\rho vH)}{\partial \theta} + \rho uH + \rho vH \cot \theta = rQ \tag{4}$$

In these equations, the radial and tangential velocity components, the density, and pressure are represented by u, v, ρ, and p, respectively. The quantities E and H are the total energy and enthalpy, respectively, and are given by

$$E = e + \frac{1}{2}\left(u^2 + v^2\right)$$

$$H = h + \frac{1}{2}\left(u^2 + v^2\right)$$

where e and h are the internal energy and static enthalpy, respectively. The quantity Q in equation (4) is the net heat input to a volume element due to the emission and absorption of thermal energy and is discussed in a subsequent section.

Equations (1) to (4) are indeterminate on the axis where the tangential component of velocity v vanishes and $\cot \theta$ is infinite. The indeterminate forms can be evaluated with the aid of l'Hospital's rule to yield the following equations:

Continuity:

$$\frac{\partial(\rho r)}{\partial t} + \frac{\partial(\rho ur)}{\partial r} + 2\frac{\partial(\rho v)}{\partial \theta} + \rho u = 0 \tag{5}$$

Radial momentum:

$$\frac{\partial(\rho ur)}{\partial t} + \frac{\partial\left[\left(p + \rho u^2\right)r\right]}{\partial r} + 2\frac{\partial(\rho uv)}{\partial \theta} - \left(p - \rho u^2\right) = 0 \tag{6}$$

Energy:

$$\frac{\partial(\rho Er)}{\partial t} + \frac{\partial(\rho uHr)}{\partial r} + 2\frac{\partial(\rho vH)}{\partial \theta} + \rho uH = rQ \tag{7}$$

The tangential momentum equation is not needed at $\theta = 0$ because the tangential velocity component is zero on the axis.

Equations (1) to (7) can be written in index notation as:

$$\frac{\partial A_i}{\partial t} + \frac{\partial B_i}{\partial r} + (1 + \mu)\frac{\partial C_i}{\partial \theta} + D_i + (1 - \mu)E_i \cot \theta = F_i \qquad (i = 1,2,3,4) \tag{8}$$

where

$$\left.\begin{array}{ll} \mu = 0 & (\theta \neq 0) \\ \mu = 1 & (\theta = 0) \end{array}\right\} \quad (9)$$

and where

$$\left.\begin{array}{ll} A_1 = \rho r & A_2 = \rho u r \\ B_1 = \rho u r & B_2 = (p + \rho u^2) r \\ C_1 = \rho v & C_2 = \rho u v \\ D_1 = \rho u & D_2 = -p + \rho(u^2 - v^2) \\ E_1 = \rho v & E_2 = \rho u v \\ F_1 = 0 & F_2 = 0 \\ A_3 = \rho v r & A_4 = \rho\left[e + \frac{1}{2}(u^2 + v^2)\right] r \\ B_3 = \rho u v r & B_4 = \rho u\left[h + \frac{1}{2}(u^2 + v^2)\right] r \\ C_3 = p + \rho v^2 & C_4 = \rho v\left[h + \frac{1}{2}(u^2 + v^2)\right] \\ D_3 = 2\rho u v & D_4 = \rho u\left[h + \frac{1}{2}(u^2 + v^2)\right] \\ E_3 = \rho v^2 & E_4 = \rho v\left[h + \frac{1}{2}(u^2 + v^2)\right] \\ F_3 = 0 & F_4 = Qr \end{array}\right\} \quad (10)$$

New independent variables are introduced as follows:

$$\tau = t \quad (11a)$$

$$\Theta = \theta \tag{11b}$$

$$Y = \frac{r - r_b}{\delta} \tag{11c}$$

where

$$\delta = \delta(\theta,t) = r_s(\theta,t) - r_b \tag{12}$$

The quantity $r_s(\theta,t)$ is the radial coordinate of the shock wave for particular values of θ and t, and r_b is the radius of the sphere. Equations (8) are written in terms of these independent variables as

$$\frac{\partial A_i}{\partial \tau} + \frac{1}{\delta}\left\{\frac{\partial B_i}{\partial Y} - Y\left[W\frac{\partial A_i}{\partial Y} + (1+\mu)\frac{\partial \delta}{\partial \Theta}\frac{\partial C_i}{\partial Y}\right]\right\} + (1+\mu)\frac{\partial C_i}{\partial \Theta}$$

$$+ D_i + (1-\mu)E_i \cot\Theta = F_i \qquad (i = 1,2,3,4) \tag{13}$$

where the component of the shock velocity normal to the body is given by

$$W = \frac{\partial \delta}{\partial \tau} \tag{14}$$

The partial differential equations (13) are approximated with finite-difference equations at points within the shock layer. These finite-difference equations and the known solution at time τ are used to determine the density ρ, the internal energy e, and the velocity components u and v at time $\tau + \Delta\tau$. The pressure p must be determined from an equation of state as a function of ρ and e. The static enthalpy h is defined by the equation

$$h = e + \frac{p}{\rho} \tag{15}$$

In order to determine the equation of state, it is convenient to define the thermodynamic function $\tilde{\gamma}(\rho,e)$ as the ratio of static enthalpy to internal energy:

$$\tilde{\gamma}(\rho,e) = \frac{h}{e} \tag{16}$$

By use of equations (15) and (16), the required equation of state is given by

$$p = \rho e(\tilde{\gamma} - 1) \tag{17}$$

It follows that

$$\left.\begin{aligned} e &= \frac{1}{\tilde{\gamma} - 1}\frac{p}{\rho} \\ h &= \frac{\tilde{\gamma}}{\tilde{\gamma} - 1}\frac{p}{\rho} \end{aligned}\right\} \tag{18}$$

Equations (17) and (18) are the same as the calorically perfect gas relations when $\tilde{\gamma}$ is replaced by the ratio of specific heats γ. However, equations (17) and (18) are true for all gases, regardless of the thermodynamic state.

Method of solution.- Let k, l, and m be the grid indices for the τ, Y, and Θ coordinates, respectively. The computational grid associated with these coordinates is shown in figure 1. As the figure indicates, a staggered grid is used.

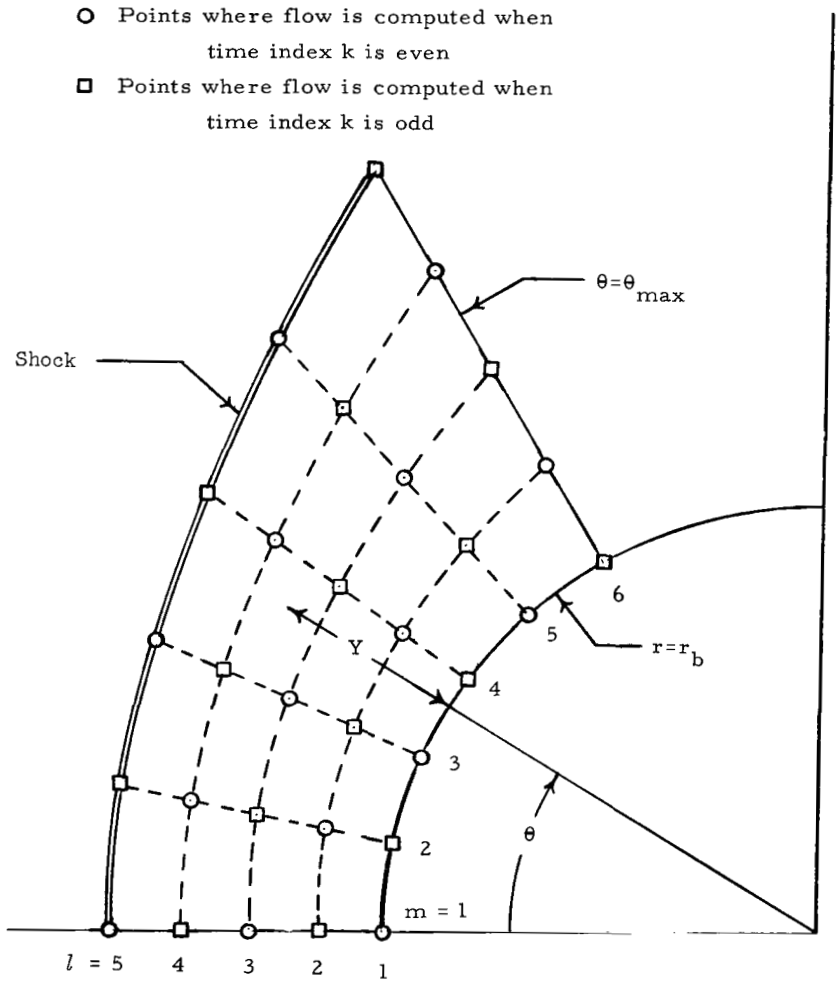

Figure 1.- Floating coordinate system.

The partial derivatives $\partial A_i/\partial\tau$ in equations (13) are replaced by forward differences as follows:

$$\left(\frac{\partial A_i}{\partial \tau}\right)^k_{l,m} = \frac{1}{\Delta\tau}\left\{(A_i)^{k+1}_{l,m} - \frac{1}{4}\left[(A_i)^k_{l+1,m} + (A_i)^k_{l-1,m} + (A_i)^k_{l,m+1} + (A_i)^k_{l,m-1}\right]\right\} + O(\Delta) \qquad (19)$$

These difference expressions contain "artificial viscosity" error terms of first order which serve to stabilize the numerical calculations. The partial derivatives $\partial B_i/\partial Y$ and $\partial C_i/\partial\Theta$ at the point (k,l,m) are replaced by central differences of the form

$$\left(\frac{\partial B_i}{\partial Y}\right)^k_{l,m} = \frac{1}{2\,\Delta Y}\left[(B_i)^k_{l+1,m} - (B_i)^k_{l-1,m}\right] + O(\Delta^2) \qquad (20a)$$

$$\left(\frac{\partial C_i}{\partial \Theta}\right)^k_{l,m} = \frac{1}{2\,\Delta\Theta}\left[(C_i)^k_{l,m+1} - (C_i)^k_{l,m-1}\right] + O(\Delta^2) \qquad (20b)$$

The difference expressions for the derivatives $\partial A_i/\partial Y$ and $\partial C_i/\partial Y$ are similar to those for $\partial B_i/\partial Y$.

Since a staggered grid is used, the flow properties are not known at the point (k,l,m). Therefore, the undifferentiated terms D_i and E_i are replaced by the averages of the values of these quantities at the neighboring grid points:

$$(D_i)^k_{l,m} = \frac{1}{4}\left[(D_i)^k_{l+1,m} + (D_i)^k_{l-1,m} + (D_i)^k_{l,m+1} + (D_i)^k_{l,m-1}\right] + O(\Delta^2) \qquad (21a)$$

$$(E_i)^k_{l,m} = \frac{1}{4}\left[(E_i)^k_{l+1,m} + (E_i)^k_{l-1,m} + (E_i)^k_{l,m+1} + (E_i)^k_{l,m-1}\right] + O(\Delta^2) \qquad (21b)$$

The terms F_i are all zero except F_4 which is equal to rQ. The treatment of this term is discussed in the section "Radiative Transfer." The expressions in equations (19), (20), and (21) and the values of the terms F_i are substituted into equations (13), and the quantities δ, W, and $\partial\delta/\partial\Theta$ are evaluated at the point (k,l,m). All the terms in the resulting finite-difference equations have a time index k except the quantities $(A_i)^{k+1}_{l,m}$. Therefore, values for A_i terms at time $k+1$ can be evaluated if the solution at time k is known.

The velocity components $u_{l,m}^{k+1}$ and $v_{l,m}^{k+1}$, the density $\rho_{l,m}^{k+1}$, and the internal energy $e_{l,m}^{k+1}$ are determined from the quantities $(A_i)_{l,m}^{k+1}$. Then the function $\tilde{\gamma}_{l,m}^{k+1}$ is evaluated in terms of $\rho_{l,m}^{k+1}$ and $e_{l,m}^{k+1}$. The method by which this is done is discussed later in the section "Thermodynamic Models." Values for the pressure $p_{l,m}^{k+1}$ and the static enthalpy $h_{l,m}^{k+1}$ are determined from equations (17) and (18), respectively.

It is seen from equations (10) that the radial coordinate r must be known at the point $(k+1, l, m)$. The equation for r is

$$r_{l,m}^{k+1} = r_b + Y\delta_m^{k+1}$$

Since the shock-layer thickness δ_m^{k+1} appears on the right-hand side of this equation, the solution at the shock at time $k + 1$ must be determined first.

The solutions at the boundary $\Theta = \Theta_{max}$ which lies downstream of both the sonic line and limiting characteristic are determined by extrapolating the flow properties linearly. The errors incurred by the extrapolation do not affect the solution upstream of the boundary because the flow in the vicinity of the boundary is supersonic.

Stability analysis.- A linear stability analysis of the finite-difference equations (13) has been performed by using the method of Von Neumann (ref. 13). The purpose of the resulting stability conditions is to insure that the magnitudes of the infinitesimal errors which are introduced at a given time step do not increase with time. Von Neumann showed that these errors are wavelike in nature. Although the quantities of interest are the sums of the errors affecting the various flow properties, the stability conditions are developed by considering the growth of only one error term for each flow property.

The Von Neumann conditions for the finite-difference equations employed in this report are

$$\frac{\Delta\tau}{\Delta Y} \leq \frac{\sqrt{2}}{2} \frac{\delta}{|u - YW| + a}$$

$$\frac{\Delta\tau}{\Delta\Theta} \leq \frac{\sqrt{2}}{2} \frac{r_b + Y\delta}{|v| + a}$$

where a is the speed of sound. The derivation of these inequalities is given in reference 14. It should be noted that these conditions are more restrictive than the

Courant-Friedrichs-Lewy conditions (ref. 15), which do not include the factor $\sqrt{2}/2$ on the right-hand side.

Calculations at Points on the Shock Wave

Governing equations.- An orthogonal curvilinear coordinate system η, ξ is established at the shock wave as shown in figure 2, where η and ξ are the distances along and normal to the shock, respectively, at time $\tau + \Delta\tau$. The velocity components in the ξ and η directions are U and V, respectively. The angle ϵ between the normal to the shock and the radial line through the point being computed is determined from the relation

$$\tan \epsilon = \frac{\partial \delta / \partial \Theta}{r_b + \delta} \tag{22}$$

The equations which must be solved at the shock wave are the Rankine-Hugoniot relations and one characteristic compatibility relation. If the subscripts ∞ and s represent quantities in the free stream and immediately behind the shock, respectively, the Rankine-Hugoniot relations can be written as

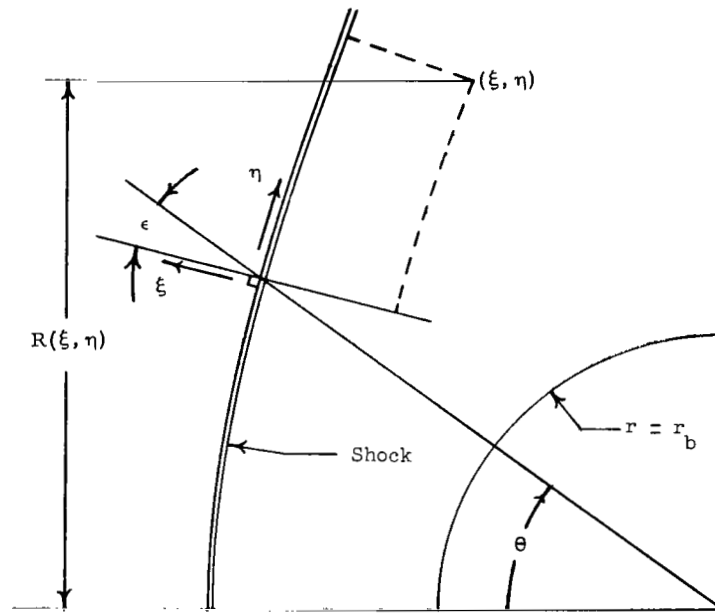

Figure 2.- Shock-oriented coordinate system.

$$\left.\begin{aligned}
&\rho_s\left(U_s - \frac{W}{\cos \epsilon}\right) = \rho_\infty\left(U_\infty - \frac{W}{\cos \epsilon}\right) \\
&p_s + \rho_s\left(U_s - \frac{W}{\cos \epsilon}\right)^2 = p_\infty + \rho_\infty\left(U_\infty - \frac{W}{\cos \epsilon}\right)^2 \\
&\frac{\tilde{\gamma}_s}{\tilde{\gamma}_s - 1}\frac{p_s}{\rho_s} + \frac{1}{2}\left(U_s - \frac{W}{\cos \epsilon}\right)^2 = \frac{\tilde{\gamma}_\infty}{\tilde{\gamma}_\infty - 1}\frac{p_\infty}{\rho_\infty} + \frac{1}{2}\left(U_\infty - \frac{W}{\cos \epsilon}\right)^2 \\
&V_s = V_\infty
\end{aligned}\right\} \tag{23}$$

The compatibility relation, which is a linear combination of the governing partial differential equations (ref. 16), is given by the equation

$$\frac{dp}{d\tau} + \rho a \frac{dU}{d\tau} = -\frac{1}{h_\eta}\left(\rho a V \frac{\partial U}{\partial \eta} + \rho a^2 \frac{\partial V}{\partial \eta} + V \frac{\partial p}{\partial \eta}\right) - \frac{1}{h_\eta}\left[\rho a^2 U\left(K + h_\eta \frac{1}{R} \sin \beta\right) + \rho a^2 V h_\eta \frac{1}{R} \cos \beta - K \rho a V^2\right] + \left[\tilde{\gamma} - 1 + \left(\frac{\partial \tilde{\gamma}}{\partial \log_e e}\right)_\rho\right] Q \tag{24}$$

where the angle between the normal to the shock wave and the free-stream direction β, the curvature of the shock wave K, and the scale factor for the η coordinate h_η are given by the equations

$$\beta(\eta) = \Theta - \epsilon$$

$$K(\eta) = \frac{\partial \beta}{\partial \eta}$$

$$h_\eta(\eta, \xi) = 1 + K\xi$$

The perpendicular distance from the axis to the point η, ξ is given by the equation

$$R(\eta, \xi) = \int_{\tilde{\eta}=0}^{\tilde{\eta}=\eta} \cos \beta(\tilde{\eta})\, d\tilde{\eta} + \xi \sin \beta(\eta)$$

where $\eta = 0$ at the axis. Two of the undifferentiated terms on the right-hand side of equation (24) are indeterminate on the axis where $\sin \beta$, V, and R are equal to zero. With the aid of l'Hospital's rule, the compatibility relation on the axis can be written as

$$\frac{dp}{d\tau} + \rho a \frac{dU}{d\tau} = -\frac{2}{h_\eta}\left(\rho a^2 \frac{\partial V}{\partial \eta} + K \rho a^2 U\right) + \left[\tilde{\gamma} - 1 + \left(\frac{\partial \tilde{\gamma}}{\partial \log_e e}\right)_\rho\right] Q \tag{25}$$

It should be noted that the form of the energy equation which is used to obtain the compatibility relation is written as

$$\frac{dp}{d\tau} - a^2 \frac{d\rho}{d\tau} = \left[\tilde{\gamma} - 1 + \left(\frac{\partial \tilde{\gamma}}{\partial \log_e e}\right)_\rho\right] Q \tag{26}$$

where the speed of sound is given by the equation

$$a^2 = e\left\{(\tilde{\gamma} - 1)\left[\tilde{\gamma} + \left(\frac{\partial \tilde{\gamma}}{\partial \log_e e}\right)_\rho\right] + \left(\frac{\partial \tilde{\gamma}}{\partial \log_e \rho}\right)_e\right\} \tag{27}$$

Equations (26) and (27) are derived in appendix A.

The compatibility relation is integrated along the line of intersection of the ξ,τ plane which passes through the shock point at time $\tau + \Delta\tau$ and the characteristic surface which passes through the shock point and intersects the η,ξ plane behind the shock wave at time τ. This line of intersection has the slope

$$\frac{d\xi}{d\tau} = U + a \tag{28}$$

in the ξ,τ plane.

Method of solution.- The solution is known completely at time τ and at all previous times. A first approximation to the shock-wave geometry at time $\tau + \Delta\tau$ is made by using the relation

$$\delta(\Theta,\tau + \Delta\tau) = \delta(\Theta,\tau - \Delta\tau) + 2W(\Theta,\tau - \Delta\tau)\Delta\tau$$

and the component of the shock velocity normal to the body is approximated by

$$W(\Theta,\tau + \Delta\tau) = W(\Theta,\tau - \Delta\tau)$$

The derivative $\partial\delta/\partial\Theta$ is computed from the equation

$$\frac{\partial \delta}{\partial \Theta} = \frac{\delta(\Theta + 2\,\Delta\Theta,\tau + \Delta\tau) - \delta(\Theta - 2\,\Delta\Theta,\tau + \Delta\tau)}{4\,\Delta\Theta} \tag{29}$$

and the angle ϵ is determined from equation (22). Tentative values for the velocity components U_s and V_s and the equilibrium thermodynamic properties ρ_s, p_s, e_s, h_s, a_s, and $\tilde{\gamma}_s$ at time $\tau + \Delta\tau$ are obtained by using the approximate value for $W(\Theta,\tau + \Delta\tau)$ and iterating the Rankine-Hugoniot relations (23), equations (18) and (27), and the equation for $\tilde{\gamma}(\rho,e)$.

At this point, the location of the line along which the compatibility relation is to be integrated is determined. The slope of this line, which lies in the ξ,τ plane and passes through the point s, is given by equation (28). The ξ,τ plane is shown in figure 3.

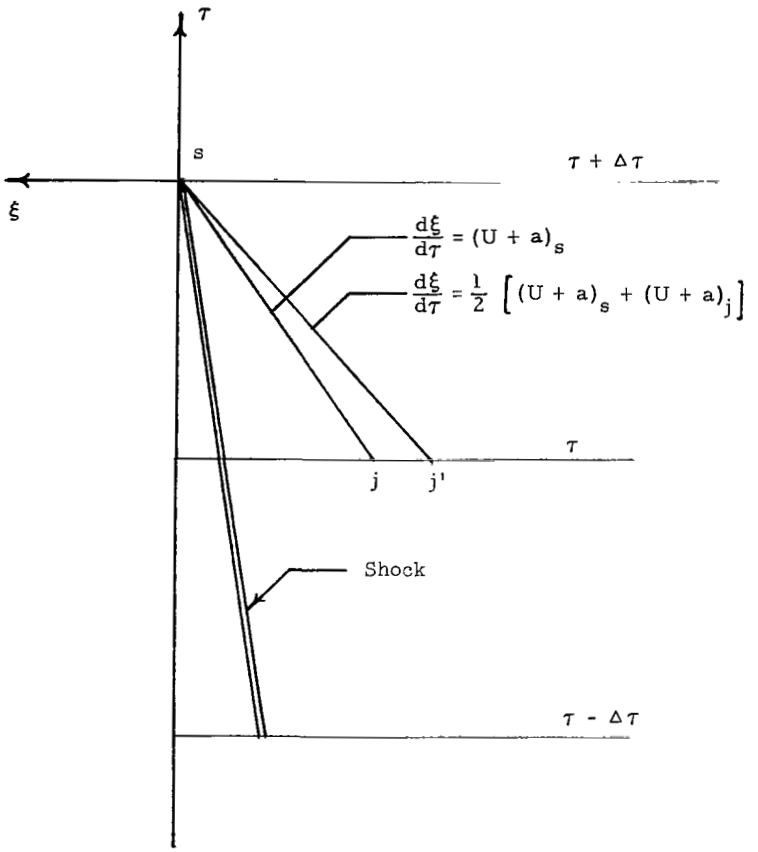

Figure 3.- Location of line along which compatibility equation is integrated.

The first estimate of the location of the point j where the line intersects the η,ξ plane at time τ is obtained by using the relation

$$\xi_j = -(U + a)_s \, \Delta\tau$$

where ξ is equal to zero at the shock, and its positive direction is outward into the free stream, as shown in figure 3. The mesh spacing $\Delta\tau$ is always positive. The values of the flow properties at point j are determined by interpolation, and ξ_j is computed again from the relation

$$\xi_j = -\frac{1}{2}\left[(U + a)_s + (U + a)_i\right]\Delta\tau$$

so that a new location for point j is determined. This process is repeated until the successive values for ξ_j converge.

The compatibility relation given by equation (24) or equation (25) is integrated from point j to point s. In order to perform this integration, the right-hand side of

equation (24) or (25) and the term ρa on the left-hand side are evaluated at s and j, and the results are averaged. The integrated compatibility relation, the Rankine-Hugoniot relations, and the thermodynamic relations are solved iteratively for the velocity components, the thermodynamic properties, and the shock velocity component W at the shock point at time $\tau + \Delta\tau$.

The next approximation of the shock-wave geometry at time $\tau + \Delta\tau$ is determined by using the relation

$$\delta(\Theta,\tau + \Delta\tau) = \delta(\Theta,\tau - \Delta\tau) + \left[W(\Theta,\tau + \Delta\tau) + W(\Theta,\tau - \Delta\tau)\right] \Delta\tau \tag{30}$$

The process given by equations (29) to (30) is repeated until the successive solutions converge.

Calculations at Points on Body Surface

Governing equations.- The transient spherical polar coordinate system r,θ,t is used to obtain solutions at the surface of the sphere. The differential equations which are solved are the energy equation (26), the tangential momentum equation, and a characteristic compatibility relation. Both the energy equation and the momentum equation are integrated along the body streamline, which has the slope

$$\frac{d\theta}{dt} = \frac{v}{r_b} \tag{31}$$

in the θ,t surface. Equation (26) is used in the form given, whereas the momentum equation is used in the form

$$\frac{dv}{dt} = -\frac{1}{\rho r}\frac{\partial p}{\partial \theta} \tag{32}$$

The compatibility relation is integrated along the line of intersection of the r,t plane (θ = Constant) which passes through the body point where the flow is being computed at time $t + \Delta t$ and the characteristic surface which passes through the body point and intersects the r,θ plane within the shock layer at time t. This line of intersection has the slope

$$\frac{dr}{dt} = u - a \tag{33}$$

in the r,t plane. The characteristic compatibility relation to be used at the body surface is

$$\frac{dp}{dt} - \rho a \frac{du}{dt} = \frac{1}{r}\left(\rho a v \frac{\partial u}{\partial \theta} - \rho a^2 \frac{\partial v}{\partial \theta} - v \frac{\partial p}{\partial \theta}\right) - \frac{1}{r}\left(2\rho a^2 u + \rho a^2 v \cot \theta + \rho a v^2\right) + \left[\tilde{\gamma} - 1 + \left(\frac{\partial \tilde{\gamma}}{\partial \log_e e}\right)_\rho\right] Q \tag{34}$$

for points off the axis of symmetry and

$$\frac{dp}{dt} - \rho a \frac{du}{dt} = -\frac{2}{r}\left(\rho a^2 \frac{\partial v}{\partial \theta} + \rho a^2 u\right) + \left[\tilde{\gamma} - 1 + \left(\frac{\partial \tilde{\gamma}}{\partial \log_e e}\right)_\rho\right] Q \tag{35}$$

at the stagnation point.

Method of solution.- A first approximation to the solution at time $\tau + \Delta\tau$ (which is the same as $t + \Delta t$ since $\tau = t$) is obtained by integrating equations (13), the partial differential equations which are used at points in the flow field. Let k, $l = 1$, and m be the indices of the body point w for the τ, Y, and Θ coordinates, respectively. The partial derivatives $\partial A_i/\partial\tau$ and $\partial B_i/\partial Y$ in equations (13) are approximated by finite-difference expressions of the form

$$\left(\frac{\partial A_i}{\partial \tau}\right)^k_{l,m} = \frac{1}{\Delta\tau}\left\{(A_i)^{k+1}_{l,m} - \frac{1}{2}\left[(A_i)^k_{l,m+1} + (A_i)^k_{l,m-1}\right]\right\} + O(\Delta)$$

and

$$\left(\frac{\partial B_i}{\partial Y}\right)^k_{l,m} = \frac{1}{\Delta Y}\left[(B_i)^k_{l+1,m} - (B_i)^k_{l,m}\right] + O(\Delta)$$

respectively. Since $Y = 0$ at the body surface, the partial derivatives $\partial A_i/\partial Y$ and $\partial C_i/\partial Y$ need not be evaluated. The derivatives $\partial C_i/\partial\Theta$ are determined from equation (20b); and the quantities D_i and E_i are evaluated at the points k, $l = 1$, $m + 1$, and k, $l = 1$, $m - 1$, and the results are averaged.

The location of the line along which the compatibility relation is integrated is determined from equation (33). The first estimate of the location of the point j where this line intersects the r,θ plane at time t is obtained from the relation

$$r_j = r_b + a_w \Delta t \tag{36}$$

The values of the flow properties at point j are determined by interpolation, and r_j is computed again from the equation

$$r_j = r_b + \frac{1}{2}\left[a_w + (a - u)_j\right]\Delta t$$

This process is repeated until the successive values for r_j converge. The compatibility relation given by equation (34) or equation (35) is integrated from point j to point w in the same manner as described for the shock wave. Because $u = 0$ at the surface, the integration of the compatibility relation yields the new value for the pressure p_w at time $t + \Delta t$.

The location of the line along which the energy equation (26) and the tangential momentum equation (32) are integrated is determined from equation (31). When the time index k for the time plane $t + \Delta t$ is even, this line extends from the body point w at time $t + \Delta t$ to a body point $\hat{j}$ at time $t - \Delta t$; when k is odd, the line extends from point w to a body point $\hat{j}$ at time t. In other words, point $\hat{j}$ is always located on a time plane with an even index k. It can be seen from figure 1 that the set of body points at which solutions are obtained when k is even includes the stagnation point. This procedure of integrating equations (26) and (32) over one and two time intervals alternately has been found to yield better results than those which were obtained by always integrating over one time interval. The first estimate of the location of point $\hat{j}$ is determined from the relation

$$\theta_{\hat{j}} = \theta_w - \frac{2v_w}{r_b}\Delta t$$

or

$$\theta_{\hat{j}} = \theta_w - \frac{v_w}{r_b}\Delta t$$

depending upon whether k is even or odd, respectively. Successive estimates of $\theta_{\hat{j}}$ are determined from the relation

$$\theta_{\hat{j}} = \theta_w - \frac{\left(v_w + v_{\hat{j}}\right)}{r_b}\Delta t$$

or

$$\theta_{\hat{j}} = \theta_w - \frac{1}{2}\frac{\left(v_w + v_{\hat{j}}\right)}{r_b}\Delta t$$

The integration of equations (26) and (32) from point $\hat{j}$ to point w is accomplished by evaluating the right-hand sides of these equations at these points and averaging the results. The term a^2 on the left-hand side of equation (26) is evaluated in the same manner. Equation (26) yields the new value of the density ρ_w since the new value for p_w is known, and equation (32) yields the tangential velocity v_w.

The process described, starting with equation (36), is repeated until the successive solutions converge.

Thermodynamic Models

Two thermodynamic models are used in this report: an equilibrium air model and a perfect gas model. Both models use equations (17) and (18) to determine the pressure p and enthalpy h as functions of the density ρ and internal energy e. The ratio $\tilde{\gamma} = h/e$ is assumed to be constant for the perfect gas model, whereas curve fits are used to evaluate it for the equilibrium air model.

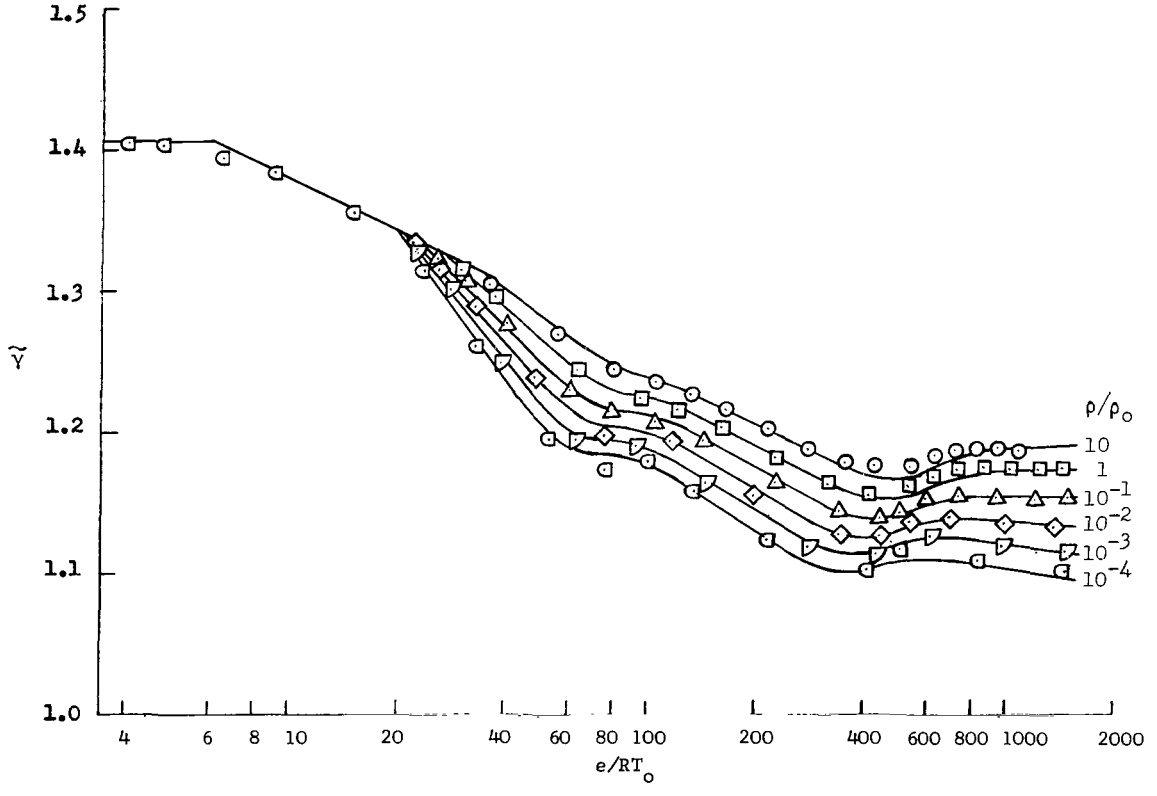

(a) Ratio of enthalpy to internal energy. Data from references 17 and 18.

Figure 4.- Curve fits of equilibrium air thermodynamic data.

Equilibrium air model.- A curve fit is used to describe the variation of the ratio $\tilde{\gamma} = h/e$ as a function of ρ/ρ_o and e/RT_o as shown in figure 4(a). The data used to construct this fit were obtained from the results of Allison (ref. 17) and Browne (ref. 18). It can be seen from the figure that for a given density, the variation of $\tilde{\gamma}$ with the logarithm of e/RT_o can be characterized by straight-line segments over most of the range $1 \leqq e/RT_o \leqq 1500$. Transitions from one straight-line segment to another occur for values of e/RT_o near 6, 25, 70, and 400. The figure shows that the transition in the vicinity of $e/RT_o = 25$ occurs rapidly, and it is assumed in this report that this transition can be approximated by an abrupt change from one straight-line segment to another. The same assumption is made with respect to the transition in the vicinity of $e/RT_o = 6$, although this transition does not occur as quickly. Transitions in the vicinity of $e/RT_o = 70$ and 400 are smooth, and they are approximated with odd transition functions (ref. 19). The curve fit for $\tilde{\gamma}$ which is used in this report is given by equations (B1) to (B4).

The curve fit which is used to determine the temperature in terms of the pressure and density is compared with the data of Browne in figure 4(b). This property is needed

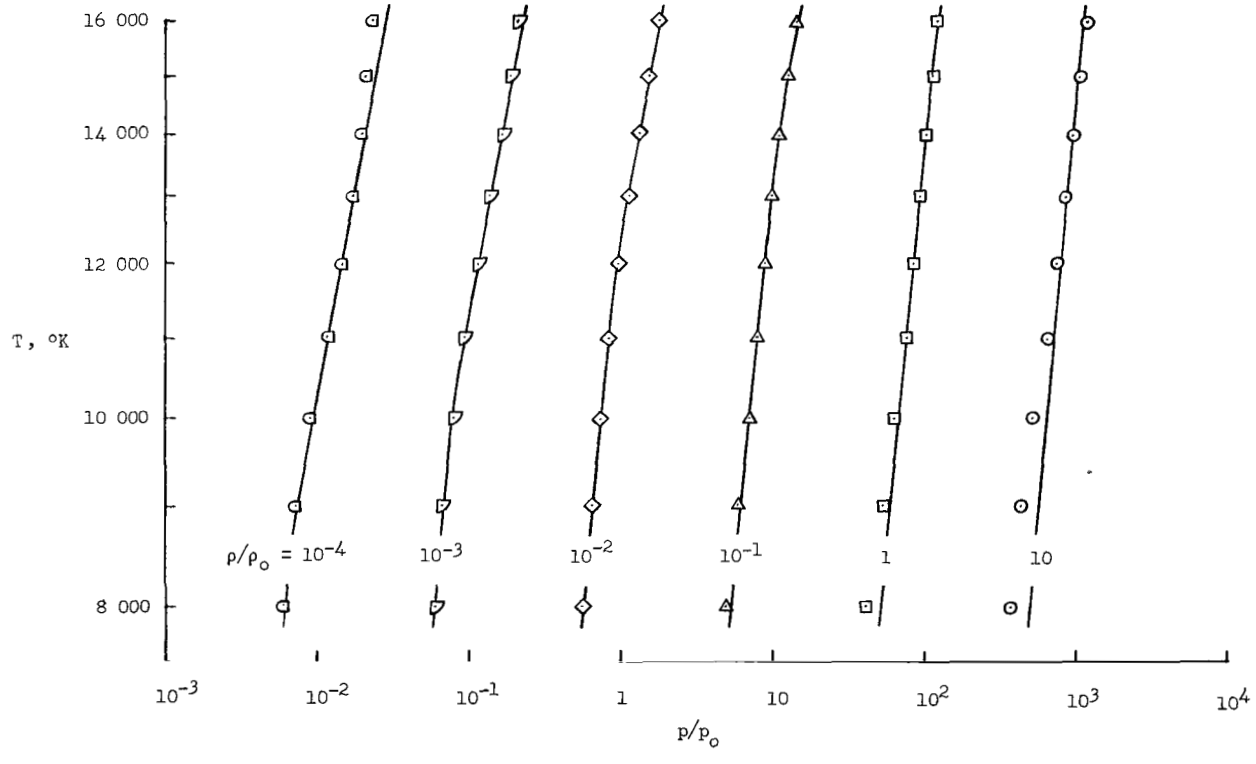

(b) Thermal equation of state. Data from reference 18.

Figure 4.- Continued.

only in connection with the computation of the heat flux and the divergence of the heat flux for the radiation problem, which are discussed in a subsequent section. The ranges of interest for the calculations in this report are

$$10^{-3} \leqq \frac{\rho}{\rho_o} \leqq 10^{-1}$$

$$8\ 000^{o}\ K \leqq T \leqq 16\ 000^{o}\ K$$

The data of Allison and Browne show that for sufficiently large values of the temperature and small values of the density within this range, the temperature can be predicted very accurately with a power-law fit of the form $T \propto p^{.432}/\rho^{.392}$. Similarly, for sufficiently small values of the temperature and large values of the density, the temperature can be predicted with a power-law fit of the form $T \propto p^{.810}/\rho^{.794}$. In this report, an even transition function (ref. 19) is used to effect the change from one power-law fit to the other. The expressions which are used in this report to determine the temperature in terms of the pressure and density are given by equations (B5) and (B6).

The speed of sound is used in the determination of the flow properties at the shock wave and the body surface. Equation (27) is used to determine the speed of sound in terms of ρ and e in this report. The derivatives of $\tilde{\gamma}$ which appear in equation (27) are obtained by differentiating the expressions for $\tilde{\gamma}$ in appendix B. The results of this procedure are compared with the data of Browne in figure 4(c).

Perfect gas model.- This model is formulated subject to the assumptions that the ratio $\tilde{\gamma} = h/e$ is constant and that the temperature is given by the equation

$$T = \frac{C_p^{\tilde{R}}}{\rho^{\tilde{S}}} \tag{37}$$

where the exponents $\tilde{R}$ and $\tilde{S}$ differ from one. It is shown in appendix C that if the entropy S is to be a conserved quantity, the ratio $\tilde{\gamma}$ and the exponents $\tilde{R}$ and $\tilde{S}$ must be related by the equation

$$1 - \tilde{S} = \tilde{\gamma}(1 - \tilde{R}) \tag{38}$$

In other words, only two of the three parameters $\tilde{\gamma}$, $\tilde{R}$, and $\tilde{S}$ can be chosen independently. It is shown also in appendix C that the speed of sound for this model is given by the relation

$$a^2 = \frac{\tilde{\gamma} p}{\rho}$$

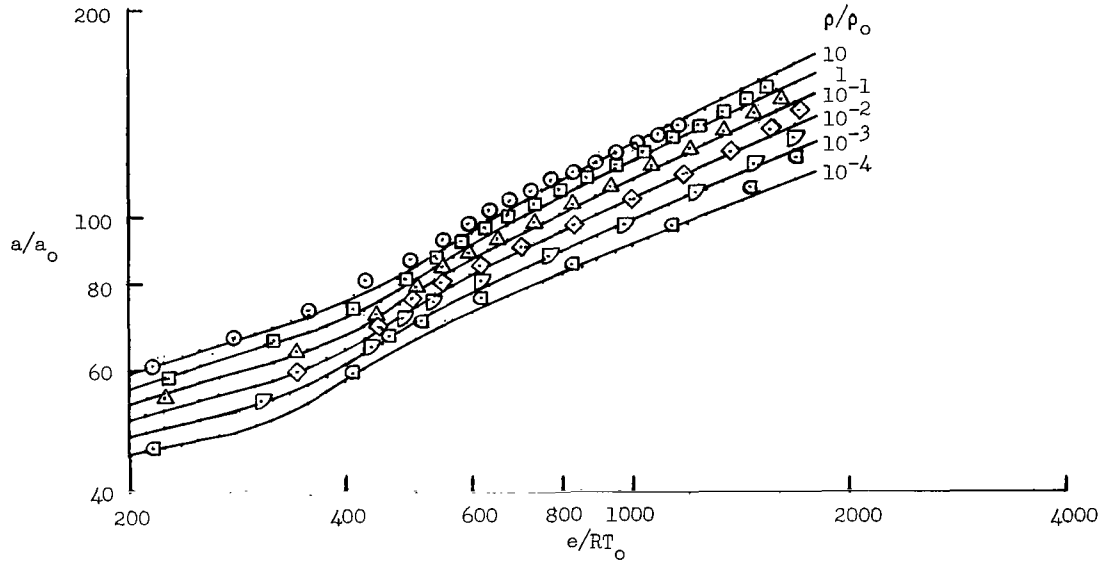

(c) Speed of sound. Data from reference 18.

Figure 4.- Concluded.

Radiative Transfer

In order to determine the amount of thermal energy which is absorbed by a fluid element, it is assumed that the radiating shock layer can be approximated by an infinite slab with the thickness of the shock layer at the point under consideration. (See fig. 5.) The distributions of the thermodynamic properties across the slab are the same as those along a normal to the surface through the point.

Both frequency-independent (gray) and frequency-dependent (nongray) absorption coefficient models are treated. The Planck mean absorption coefficient is used for the gray model, whereas a two-step coefficient is used for the nongray model. One step lies in the vacuum ultraviolet portion of the spectrum (400Å $\leqq \lambda \leqq$ 1130Å) and the other covers the near ultraviolet, visible, and infrared portions of the spectrum (1130Å $\leqq \lambda < \infty$). A Planck mean averaging procedure is used to determine the absorption coefficients for the two spectral bands.

One-dimensional radiating shock layer model.- The equation for the net addition of heat to a volume element due to monochromatic radiation can be obtained from

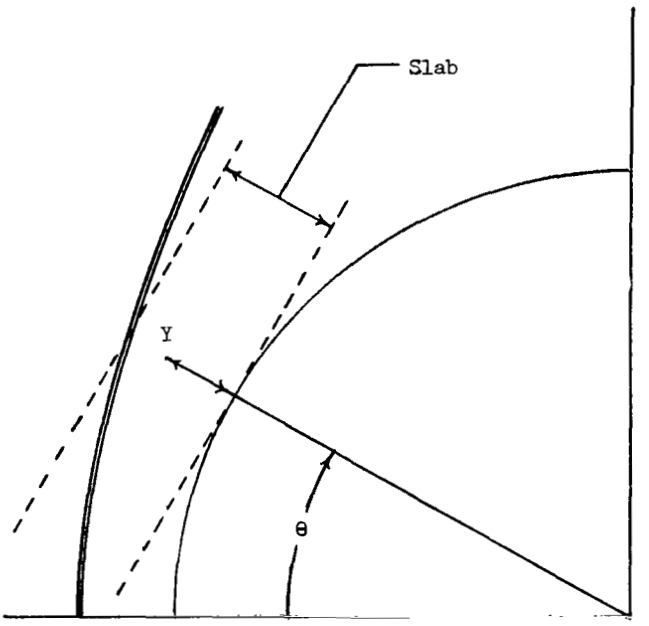

Figure 5.- Schematic of slab used for calculation of heat-flux and net-heat-input terms.

equation (D14). This equation is an expression for the net monochromatic heat input per unit volume for a one-dimensional slab. It was derived subject to the assumptions that the body surface neither reflects nor emits radiation, and that the gas in the free stream neither emits nor absorbs. The quantities $I_\nu^+(y_b)$ and $I_\nu^-(y_s)$ therefore have values of zero. When equation (D14) is substituted into equation (D15), the following expression for $Q(y)$ is obtained:

$$Q(y) = -2\pi \int_{\nu=0}^{\nu=\infty} \alpha_\nu(y)\Big(B_\nu(y_b)E_2\left[A_\nu(y_b,y)\right] + B_\nu(y_s)E_2\left[A_\nu(y,y_s)\right]$$

$$+ \int_{s=y_b}^{s=y} \frac{1}{\alpha_\nu(s)} \frac{dB_\nu}{ds} d\left\{E_3\left[A_\nu(s,y)\right]\right\} + \int_{s=y}^{s=y_s} \frac{1}{\alpha_\nu(s)} \frac{dB_\nu}{ds} d\left\{E_3\left[A_\nu(y,s)\right]\right\}\Big) d\nu$$

where B_ν is the Planck function

$$B_\nu = \frac{2h\nu^3}{c^2} \frac{1}{e^{h\nu/kT} - 1}$$

$E_n(z)$ is an exponential integral

$$E_n(z) = \int_{\omega=1}^{\omega=\infty} \frac{e^{-\omega z}}{\omega^n} d\omega \tag{39}$$

and $A_\nu(r,s)$ is the optical depth

$$A_\nu(r,s) = \int_{t=r}^{t=s} \alpha_\nu(t)dt \tag{40}$$

Consider an absorption coefficient model with M steps:

$$\alpha_\nu = \alpha_N \quad \left(\nu_N \leqq \nu \leqq \nu_{N+1}; N = 1,2,\ldots,M\right) \tag{41}$$

The integral of the Planck function over a frequency interval is given by the equation

$$\int_{\nu=\nu_N}^{\nu=\nu_{N+1}} B_\nu \, d\nu = \frac{\sigma T^4}{\pi}\left[F\left(\frac{h\nu_N}{kT}\right) - F\left(\frac{h\nu}{kT} N + 1\right)\right] \tag{42}$$

where

$$F(z) = \sum_{n=1}^{\infty} \frac{15}{\pi^4}\left(\frac{z^3}{n} + 3\,\frac{z^2}{n^2} + 6\,\frac{z}{n^3} + \frac{6}{n^4}\right)e^{-nz} \tag{43}$$

The net heat input for an M step nongray absorption coefficient model is

$$\begin{aligned} Q(y) = -2\sigma \sum_{N=1}^{M} \Bigg[& \alpha_N(y)\Bigg(T^4(y_b)\left\{F\left[\frac{h\nu_N}{kT(y_b)}\right] - F\left[\frac{h\nu_{N+1}}{kT(y_b)}\right]\right\} E_2\left[A_N(y_b,y)\right] + T^4(y_s)\left\{F\left[\frac{h\nu_N}{kT(y_s)}\right]\right. \\ & \left. - F\left[\frac{h\nu_{N+1}}{kT(y_s)}\right]\right\} E_2\left[A_N(y,y_s)\right] + \int_{s=y_b}^{s=y} \frac{1}{\alpha_N(s)} \frac{d}{ds}\Bigg(T^4(s)\left\{F\left[\frac{h\nu_N}{kT(s)}\right]\right. \\ & \left. - F\left[\frac{h\nu_{N+1}}{kT(s)}\right]\right\}\Bigg) d\left\{E_3\left[A_N(s,y)\right]\right\} + \int_{s=y}^{s=y_s} \frac{1}{\alpha_N(s)} \frac{d}{ds}\Bigg(T^4(s)\left\{F\left[\frac{h\nu_N}{kT(s)}\right]\right. \\ & \left. - F\left[\frac{h\nu_{N+1}}{kT(s)}\right]\right\}\Bigg) d\left\{E_3\left[A_N(y,s)\right]\right\}\Bigg)\Bigg] \end{aligned} \tag{44}$$

Equation (44) is used to determine the quantity Q in equations (4) and (7).

Equations (D7) and (D8) can be combined to obtain an equation for the heat flux at the body surface $q(y_b)$:

$$q(y_b) = -2\pi \int_{\nu=0}^{\nu=\infty} \left(\int_{s=y_b}^{s=y_s} B_\nu(s) d\left\{ E_3\left[A_\nu(y_b,s)\right] \right\} \right) d\nu$$

The expression for the heat flux at the surface for an infinite slab and an M step absorption coefficient model is written as

$$q(y_b) = -2\sigma \sum_{N=1}^{M} \left(\int_{s=y_b}^{s=y_s} T^4(s) \left\{ F\left[\frac{h\nu_N}{kT(s)}\right] - F\left[\frac{h\nu_{N+1}}{kT(s)}\right] \right\} d\left\{ E_3\left[A_N(y_b,s)\right] \right\} \right) \tag{45}$$

Equations (44) and (45) are integrated numerically. The absorption coefficients α_N are used in tabular form as functions of the density ρ and the temperature T.

Absorption coefficient models.- The one- and two-step models which are used in this report are constructed from the more complex models of Olstad. (See ref. 5.) The sources of radiation which are treated in that reference include the following groups: (1) atomic lines, (2) N^+ and O^+ electron recombination in the vacuum ultraviolet portion of the spectrum, and (3) molecular band systems, free-free electron transitions, the photoionization of 0, and electron recombination in the visible and infrared portions of the spectrum.

Olstad determines the absorption coefficients for electron recombination radiation in the vacuum ultraviolet portion of the spectrum from the absorption cross sections of Hahne (ref. 20). The data of Allen (refs. 21 and 22) are used to compute the absorption coefficients for the radiation sources listed in groups 1 and 3.

The step of the nongray model for the vacuum ultraviolet portion of the spectrum (400Å $\leqq \lambda \leqq$ 1130Å) accounts for the electron recombination radiation in that spectral region. The radiation from this part of the spectrum is optically thick for all the shock layers treated in this report except those associated with spheres with radii of 1 foot or less.

The second step of the nongray model accounts for the radiation due to the processes listed in group 3, the atomic lines above 2000Å, and the wings of the lines below 2000Å. The radiation due to these processes occurs in the near ultraviolet, visible, and infrared portions of the spectrum (1130Å $\leqq \lambda \leqq \infty$) and is optically thin for the cases treated in this report.

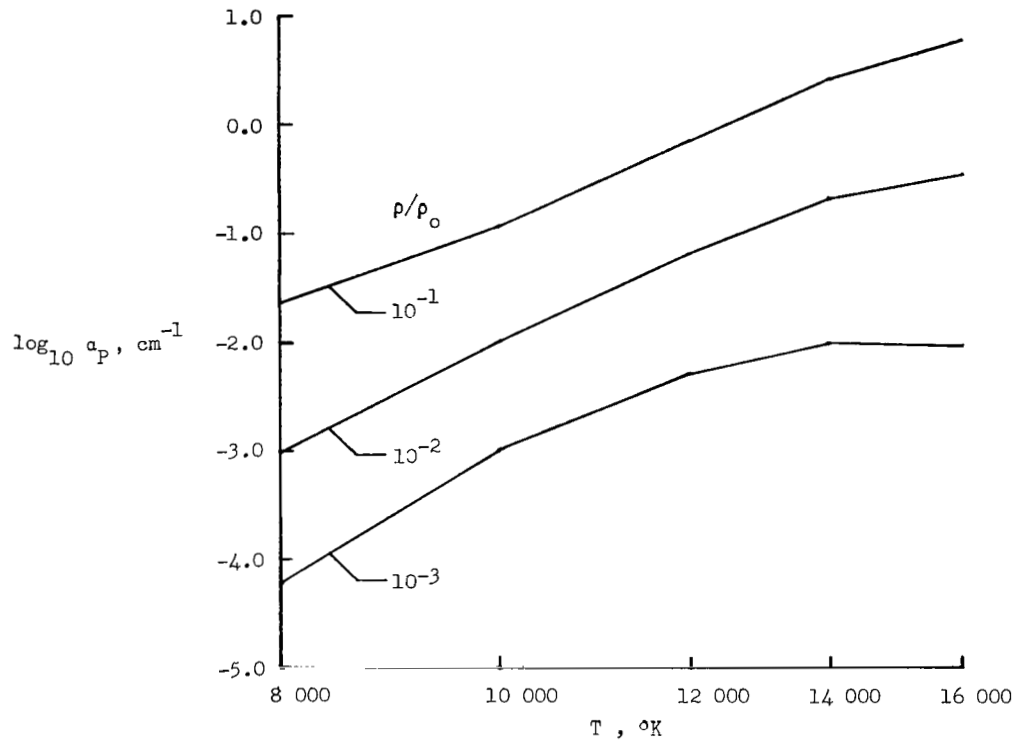

(a) Gray model.

Figure 6.- Absorption coefficients for equilibrium air.

The present model does not account for the radiation from the centers of the lines below 2000Å, which is optically thick. In order to take it into account, a model with more than two steps would have to be employed. The errors encountered by neglecting the radiation from the line centers are probably not severe since this radiation tends to be absorbed quickly.

The gray absorption coefficient model which is used in this report is shown graphically in figure 6(a), and the nongray model is shown in figure 6(b).

Starting Solution

The starting solution is constructed by specifying the shock-wave shape and surface pressure distribution. Since the shock wave is assumed to be stationary initially, the flow properties at points on the shock wave can be determined from the Rankine-Hugoniot relations. The properties at points on the body surface are determined by using the specified pressure distribution and assuming that the entropy and total enthalpy are conserved along the body streamline. The pressure and the velocity components are determined at points

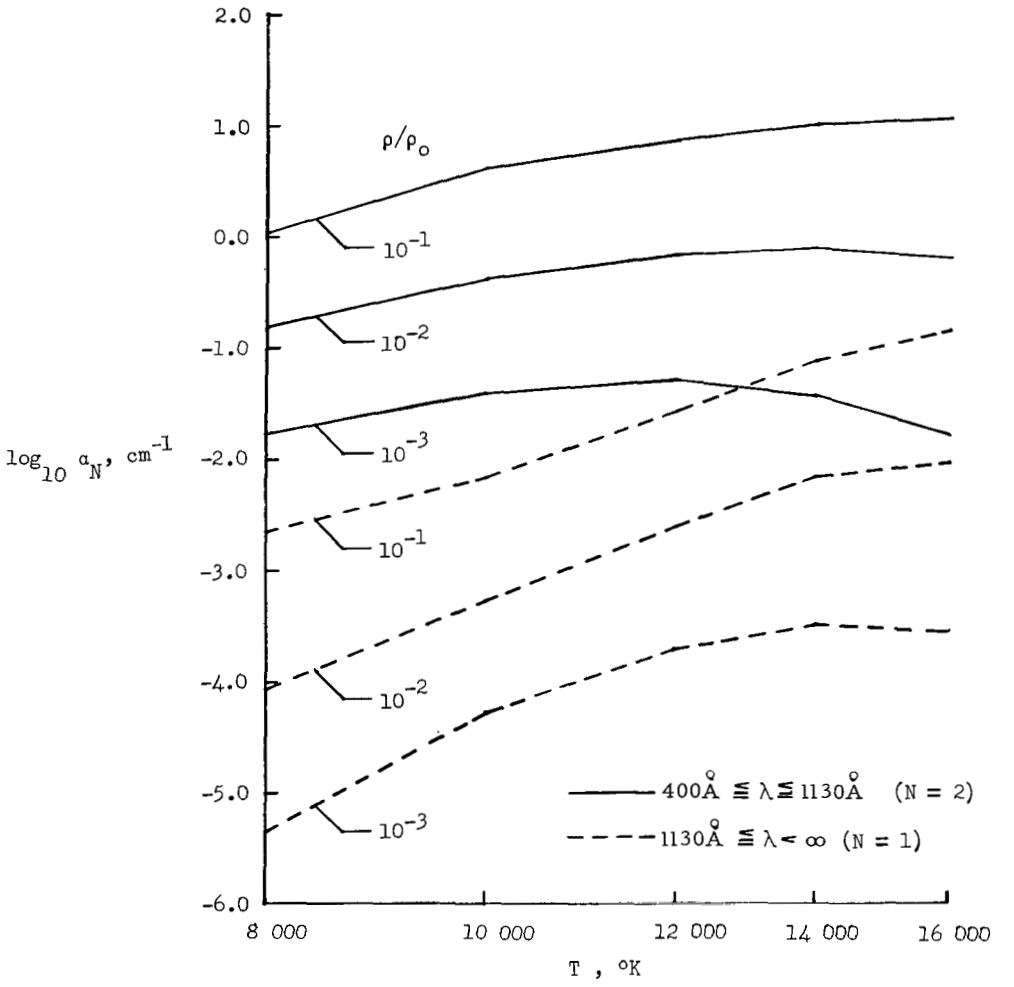

(b) Nongray model.

Figure 6.- Concluded.

within the shock layer by interpolating the values at the shock wave and body surface linearly along lines normal to the body surface. The density and enthalpy profiles along the stagnation streamline are determined with a solution similar to that used by Goulard in reference 1. This solution is developed in appendix E. Similar profiles are used along the other lines normal to the body surface. The values of the stagnation-point enthalpy which are used for the starting solution are obtained by linearly extrapolating the values at the two neighboring points on the stagnation streamline. (See appendix E.) The correct values for the cases treated in this report are much lower than the extrapolated values since a radiation-cooled layer exists at the stagnation point which is much thinner than any practical value of the mesh spacings which can be used. The use of the

correct value of the stagnation-point enthalpy would lead to an erroneous broadening of the radiation-cooled layer over several mesh spacings since the first-order computational method which is used in this report tends to reduce steep gradients in the flow property profiles such as those associated with the radiation-cooled layer. It has been found that better solutions for the flow field are obtained when the extrapolated value of the stagnation-point enthalpy is used, although the radiation-cooled layer is eliminated by this process. This procedure does not affect the value for the stagnation-point heat flux appreciably since the radiation-cooled layer is so thin. It should be noted that the present computational method adjusts the flow properties at the stagnation point much more slowly than elsewhere. Therefore, the starting solution for the stagnation streamline, and hence the extrapolated starting solution for the stagnation point, must be determined as accurately as possible.

RESULTS

In this section, calculations which are determined with the present method for both adiabatic and nonadiabatic flow are compared with those obtained with other techniques. The stagnation streamline enthalpy profiles and the shock-layer thickness distributions for spheres with different radii and the same flight conditions are shown, and the gray and the nongray surface heat-flux distributions for these spheres are compared. In addition, the effects of sphere size, free-stream velocity, and altitude on the nongray surface heating distributions are investigated. The free-stream thermodynamic properties which are used in this report are based on the atmospheric model of reference 23.

Illustrative Calculation for Adiabatic Flow

In order to demonstrate the accuracy of the present computational method and thermodynamic model, an illustrative calculation for adiabatic flow is made. The computation is made for the flow of equilibrium air past a sphere traveling at 45 000 ft/sec (13.73 km/sec) at an altitude of 200 000 ft (60.96 km) in the atmosphere of the earth. The mesh spacings which are used are $\Delta Y = 1/6$ and $\Delta\Theta = 3.875^{\circ}$.

The results of the present method are compared in figure 7 with those of Lomax and Inouye (ref. 24), who use the inverse method. It is seen in figure 7(a) that the results of the two methods for the shock-wave and sonic-line locations are in close agreement. The present method yields a value of $\delta/r_b = 0.0467$ for the stagnation streamline shock detachment distance, whereas the inverse method gives the value $\delta/r_b = 0.0479$. The results for the tangential velocity and density distributions at the surface are shown in figure 7(b). The distributions of these flow properties along a line normal to the body

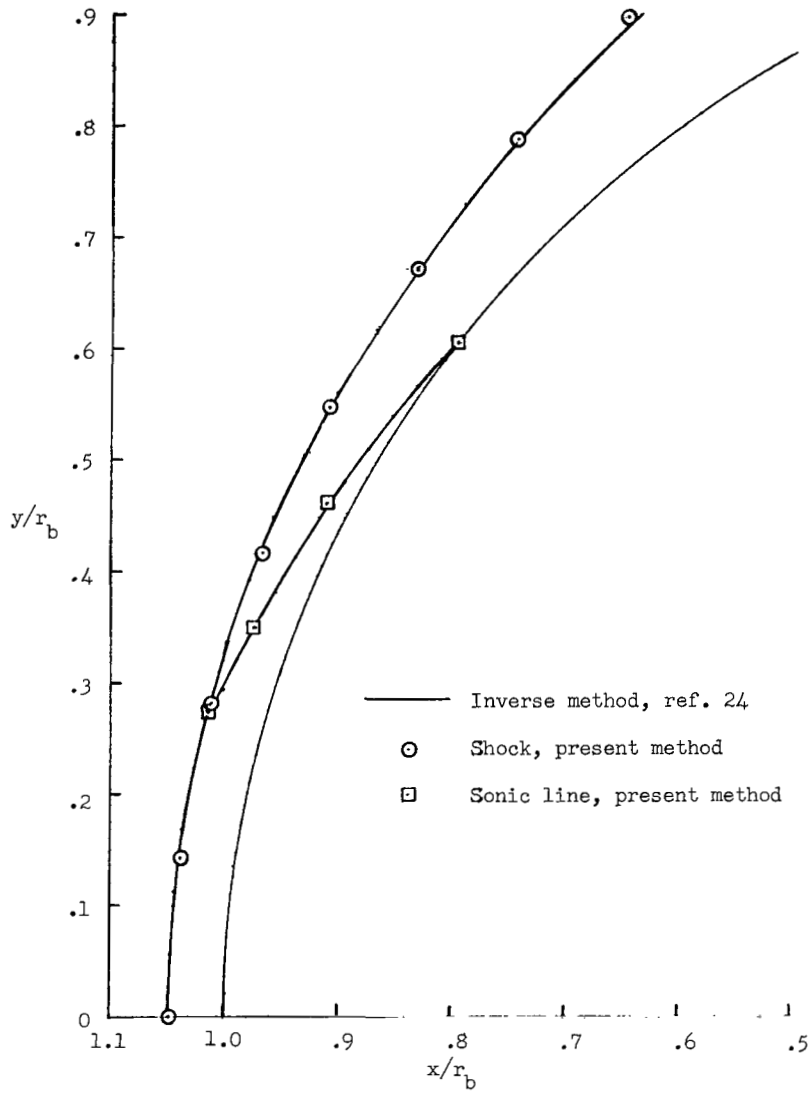

(a) Shock and sonic line locations.

Figure 7.- Adiabatic flow about a sphere traveling at 45 000 ft/sec (13.73 km/sec) at an altitude of 200 000 ft (60.96 km).

surface at $\Theta = 38.75^{\circ}$ are given in figure 7(c). It should be noted that the present method computes the density less accurately than any of the other flow properties.

Sample Calculations for Nonadiabatic Flow

The gray radiation model is used for these sample calculations. The method used to obtain the initial solutions has been discussed previously. Equations (E27) and (E29) are used to determine the initial stagnation streamline enthalpy distribution. A one-step

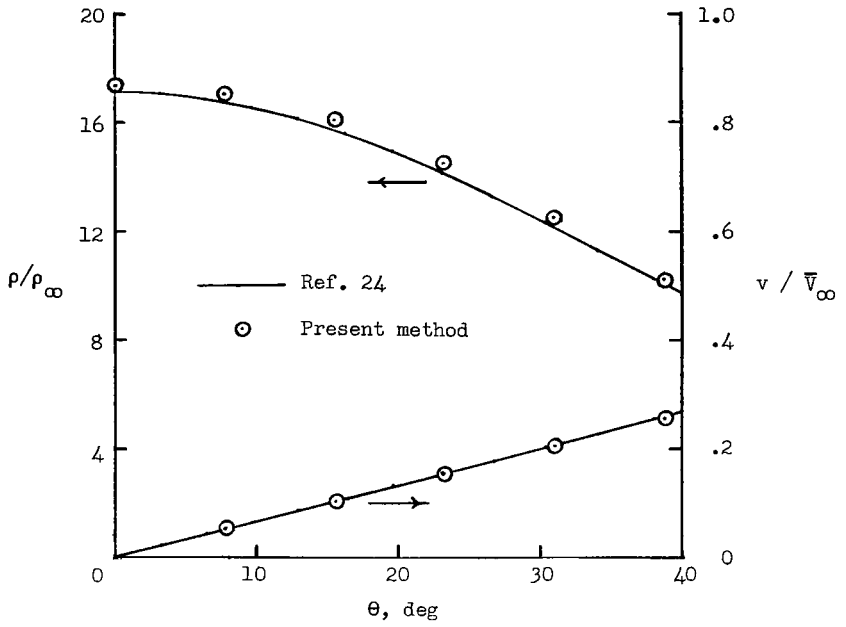

(b) Surface density and velocity distributions.

Figure 7.- Continued.

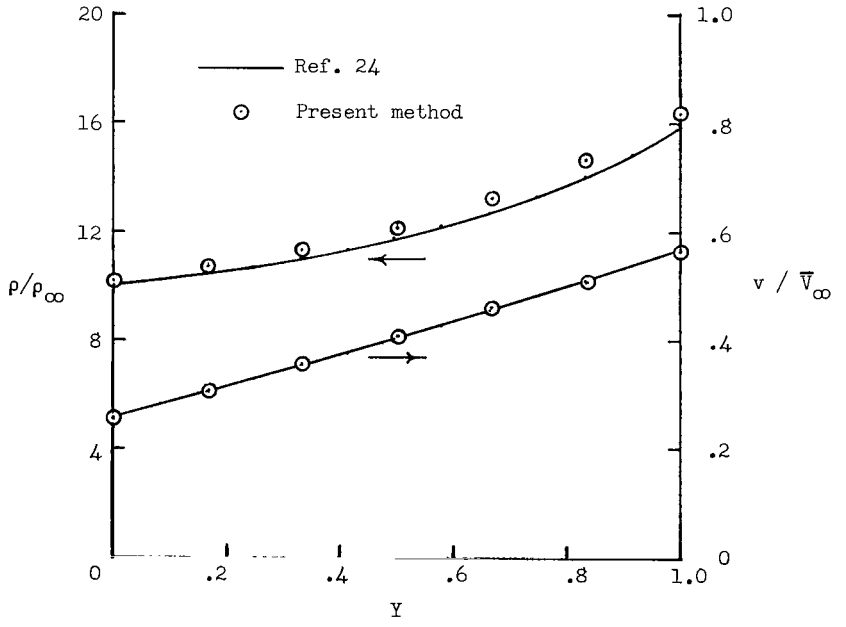

(c) Density and tangential velocity profiles across shock layer at $\theta = 38.75^0$.

Figure 7.- Concluded.

absorption coefficient which covers the spectral range $400\text{Å} \leqq \lambda < \infty$ is used for the gray radiation model. The power-law expression, which is obtained by curve fitting the data presented in figure 6(a) over the ranges $10^{-3} \leqq \frac{\rho}{\rho_o} \leqq 10^{-1}$ and $10\,000^{\circ}\text{ K} \leqq T \leqq 16\,000^{\circ}\text{ K}$, is given by the equation

$$\alpha_P = 0.3060\left(\frac{\rho}{\rho_o}\right)^{1.179}\left(\frac{T}{10^4}\right)^{6.964} \text{ cm}^{-1}$$

The dependence of temperature on enthalpy is assumed to be

$$T \propto h^{.392}$$

The constant $\tilde{C}$ in equation (E27) is set equal to zero since a one-step absorption coefficient is being considered.

Effect of mesh spacing size.- Sample calculations are made for a sphere with a radius of 5 feet (1.524 m) traveling at a speed of 50 000 ft/sec (15.24 km/sec) at an altitude of 190 000 ft (57.91 km) in the atmosphere of the earth.

The influence of the mesh spacing size on the enthalpy distribution is shown in figure 8. Calculations are presented in figure 8(a) for $\Delta Y = 1/14$ and $\Delta\Theta = 1^{\circ}$, 2°, 4°, and 6°; the solutions for the enthalpy distribution and the shock-detachment distance are seen to converge as $\Delta\Theta$ is decreased. In figure 8(b) results are shown for $\Delta\Theta = 2^{\circ}$ and $\Delta Y = 1/6$, $1/10$, $1/14$, and $1/18$; the results are seen to converge as ΔY is decreased, although the convergence is not as strong for ΔY as for $\Delta\Theta$.

The effects of the size of the mesh spacings $\Delta\Theta$ and ΔY on the surface heat-flux distribution are shown in figures 9(a) and 9(b), respectively. There is a strong tendency for these distributions to converge as the size of the mesh spacings is reduced. The results for the distributions are in close agreement for $\Delta Y = 1/14$ and $\Delta\Theta = 1^{\circ}$ and 2°. For $\Delta\Theta = 2^{\circ}$ and $\Delta Y = 1/14$ and $1/18$, the results coincide for $\Theta \leqq 30^{\circ}$ and show close agreement for $\Theta > 30^{\circ}$.

On the basis of the results presented in figures 8 and 9, the mesh spacings for the subsequent calculations are chosen to be $\Delta Y = 1/14$ and $\Delta\Theta = 1^{\circ}$.

Comparisons with other methods.- The present method has been used to calculate two cases which are presented by Olstad in reference 4. Olstad employs the optically thin approximation and uses the Poincaré-Lighthill-Kuo method to make the calculations for these cases.

The perfect-gas thermodynamic model is used to calculate the results of the present method. The free-stream pressure is set equal to zero and the quantity $\tilde{\gamma} = h/e$

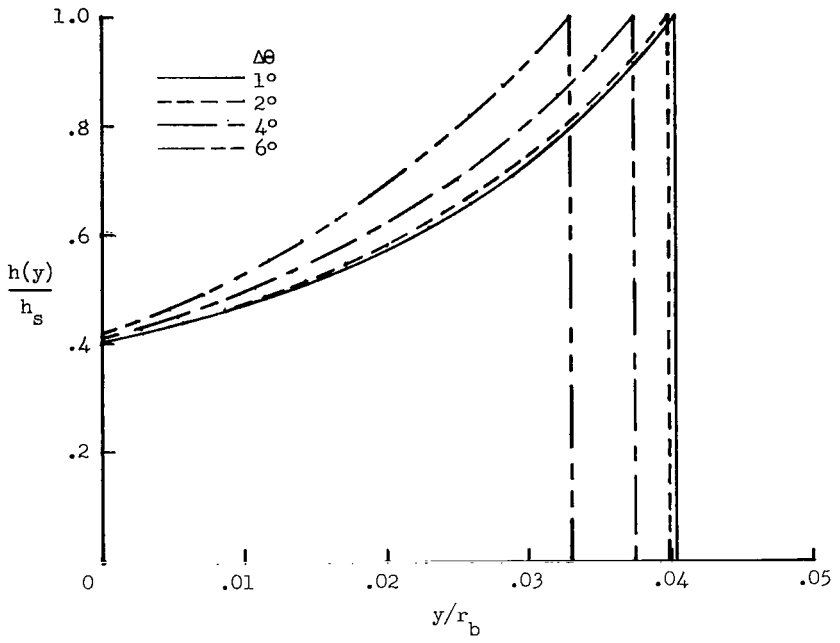

(a) Effect of $\Delta\theta$ for $\Delta Y = 1/14$.

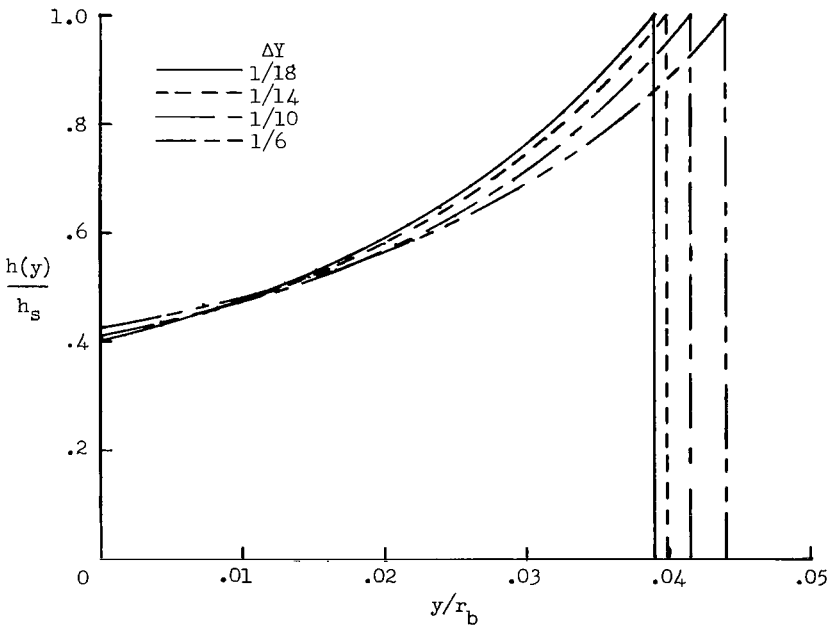

(b) Effect of ΔY for $\Delta\theta = 2^{\circ}$.

Figure 8.- Effect of mesh spacing size on gray stagnation streamline enthalpy distribution for a sphere with a radius of 5 ft (1.524 m) traveling at 50 000 ft/sec (15.24 km/sec) at an altitude of 190 000 ft (57.91 km).

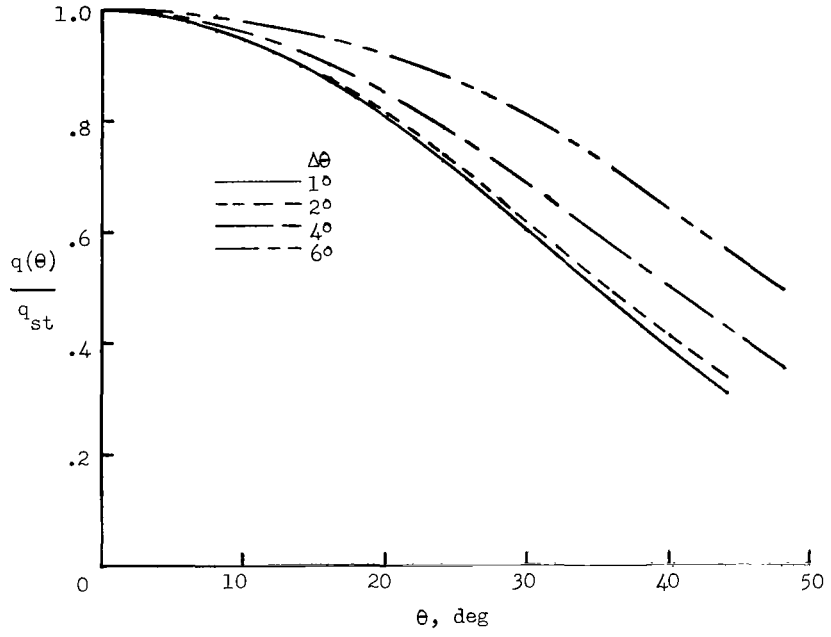

(a) Effect of $\Delta\theta$ for $\Delta Y = 1/14$.

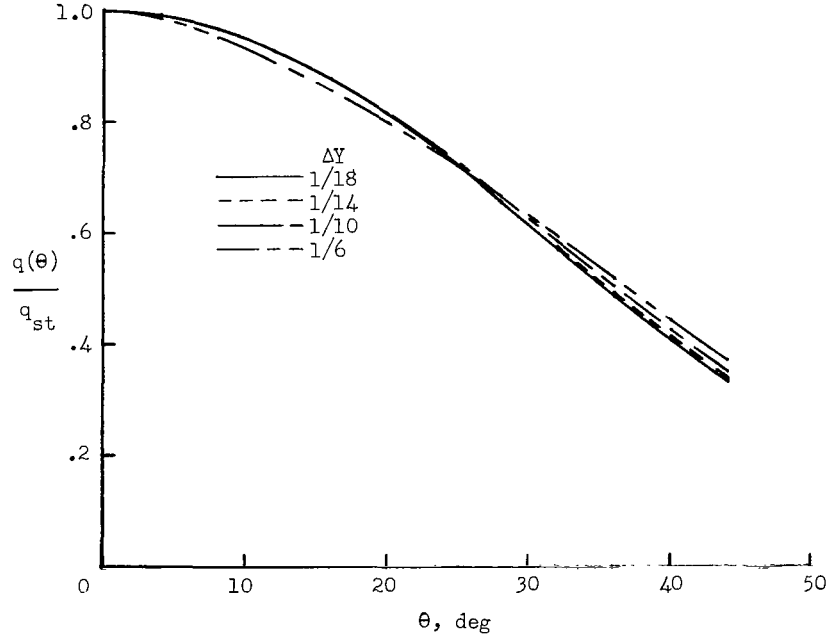

(b) Effect of ΔY for $\Delta\theta = 2^{0}$.

Figure 9.- Effect of mesh spacing size on gray surface heat-flux distributions for a sphere with a radius of 5 ft (1.524 m) traveling at 50 000 ft/sec (15.24 km/sec) at an altitude of 190 000 ft (57.91 km).

is chosen so that the density at the shock wave is $\frac{\rho_\infty}{\rho_s} = 0.06$, the value used in reference 4. The dependence of temperature on the density and pressure is of the form

$$T \propto \frac{p^{.601}}{\rho^{.550}}$$

The density exponent $\tilde{S} = 0.55$ is the same as the enthalpy exponent used in reference 4, and the pressure exponent $\tilde{R}$ was computed from equation (38). The dependence of the absorption coefficient on the density and temperature is taken to be

$$\alpha_P \sim \rho^{.661} T^{6.656}$$

Therefore, the absorption coefficient varies as h^3 when the pressure is constant. This variation was used in reference 4 for the cases which are being treated.

Let the energy depletion parameter Γ be defined by the equation

$$\Gamma = \frac{4\alpha_{P,s}\delta_A \sigma T_s^4}{\rho_\infty \bar{V}_\infty h_s} \tag{46}$$

where δ_A is the shock-detachment distance for adiabatic flow. The gases which are treated have the parameters $\alpha_{P,s}\delta_A = 0.3$, $\Gamma = 0.02$ and $\alpha_{P,s}\delta_A = 1$, $\Gamma = 2$.

The results of the present method for the stagnation streamline enthalpy profiles are compared with those of Olstad in figure 10. The agreement is reasonably good for both cases. The results of the present method for the stagnation-point heat fluxes are $\frac{q_{st}}{\rho_\infty \bar{V}_\infty^3} = 0.0032$ and 0.0632 whereas the values presented in reference 4 are 0.0028 and 0.0574. The present method gives values of $\delta = 0.994\delta_A$ and $0.797\delta_A$ for the shock-detachment distances for the two cases, whereas reference 4 gives values of $0.982\delta_A$ and $0.732\delta_A$.

The results of the present method for the surface heat-flux distribution are compared with those of Wilson and Hoshizaki (ref. 7) in figure 11. The case which is treated is a sphere with a radius of 5 feet (1.524 m) traveling at 50 000 ft/sec (15.24 km/sec) at an altitude of 190 000 ft (57.91 km) in the atmosphere of the earth. The gray radiation model is used. Two distributions from reference 7 are shown in the figure because the authors use upper bound and lower bound absorption coefficient models in that reference. It is seen that the heat-flux distribution computed by the present method is very similar to the distribution of reference 7.

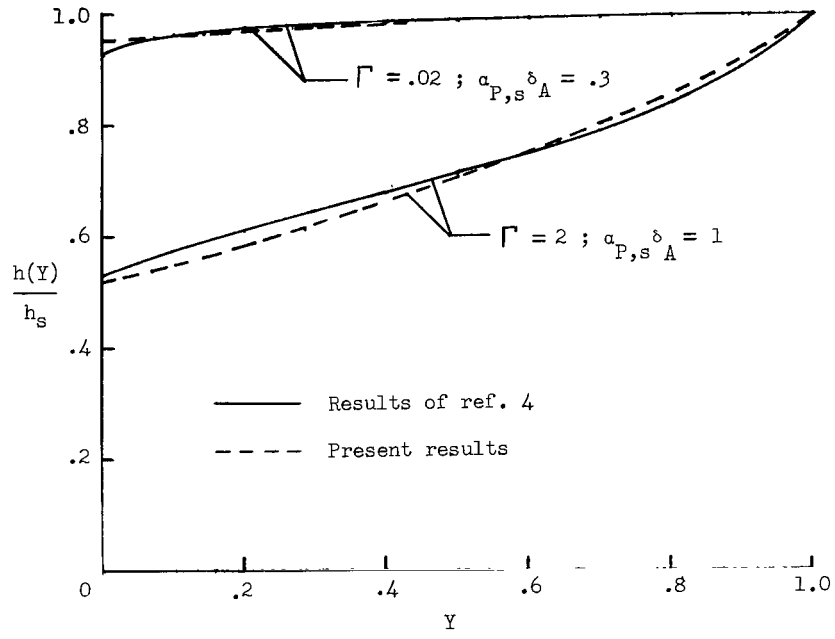

Figure 10.- Comparison of present results and those of reference 4 for gray stagnation-streamline enthalpy distribution.

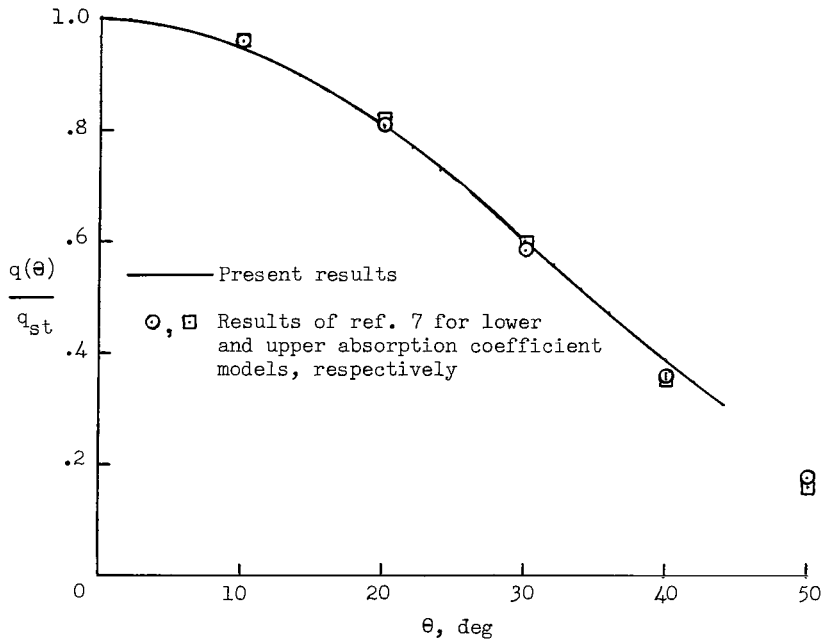

Figure 11.- Comparison of present results and those of reference 7 for gray surface heat-flux distribution for a sphere with a radius of 5 ft (1.524 m) traveling at 50 000 ft/sec (15.24 km/sec) at an altitude of 190 000 ft (57.91 km).

Calculations for Spheres With Different Radii and Different Flight Conditions

The thickness of the shock layer is roughly proportional to the radius of the body. Therefore, the body size governs the optical depth of the shock layer. The flight velocity determines the amount of energy available to the flow field, whereas the velocity and the free-stream conditions together determine the magnitudes of the flow properties behind the shock wave.

Altitude, 190 000 feet (57.91 km); velocity, 50 000 ft/sec (15.24 km/sec).- Results for spheres traveling in the atmosphere of the earth at an altitude of 190 000 feet (57.91 km) at a velocity of 50 000 ft/sec (15.24 km/sec) are presented in this section. The effects of body size on the stagnation streamline enthalpy profile, the shock-layer thickness, and the surface heat-flux distributions are investigated. Spheres with the radii of 3 inches (0.0762 meter), 1 foot (0.3048 meter), 5 feet (1.524 meters), and 15 feet (4.572 meters) are treated.

The initial solution for the gray cases has been discussed previously. A two-step absorption coefficient model is used in connection with equations (E27) and (E29) to determine the initial solution for the nongray cases. Again, the temperature is assumed to vary as $h^{.392}$. The data presented in figure 6(b) are used to obtain the power-law expressions for the absorption coefficient model. The coefficient for the step which covers the spectral range $1130\text{Å} \leqq \lambda < \infty$ is written as

$$\alpha_1 = 0.1489\left(\frac{\rho}{\rho_o}\right)^{1.163}\left(\frac{T}{10^4}\right)^{5.498} \text{ cm}^{-1} \tag{47}$$

where the temperature T is given in ^{o}K. For the cases $r_b = 3$ inches and $r_b = 1$ foot, the second step covers the spectral range $400\text{Å} \leqq \lambda \leqq 1130\text{Å}$. The power-law absorption coefficient for this range is

$$\alpha_2 = 110.9\left(\frac{\rho}{\rho_o}\right)^{1.182}\left(\frac{T}{10^4}\right)^{.469} \text{ cm}^{-1}$$

For the case with $r_b = 5$ feet, the second step covers the spectral range $1020\text{Å} \leqq \lambda \leqq 1130\text{Å}$. For this case, the radiation for $\lambda < 1020\text{Å}$ is optically thick. It is assumed that for these conditions this radiation, which is absorbed by the flow field very close to the point at which it is emitted, does not affect the structure of the flow field appreciably and can be neglected. The power-law absorption coefficient for the range $1020\text{Å} \leqq \lambda \leqq 1130\text{Å}$ is given by the expression

$$\alpha_2 = 23.11\left(\frac{\rho}{\rho_o}\right)^{1.201}\left(\frac{T}{10^4}\right)^{.845}$$

For the case with $r_b = 15$ feet, the radiation for $\lambda < 1130\text{Å}$ is optically thick and is neglected. Therefore, only one step is used for this case.

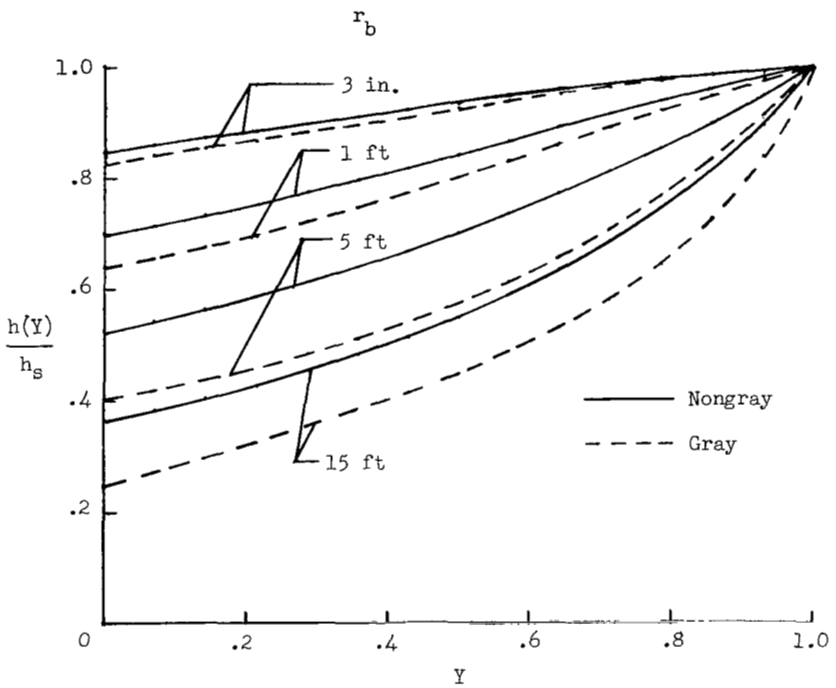

Figure 12.- Effect of size on gray and nongray stagnation-streamline enthalpy distributions for spheres traveling at 50 000 ft/sec (15.24 km/sec) at an altitude of 190 000 ft (57.91 km).

In figure 12, the enthalpy distributions along the stagnation streamline are shown for the various cases. It is seen that the effects of radiation on the enthalpy are more pronounced for the gray model than for the nongray model. As the radius of the body is increased, the differences in the gray and nongray distributions increase.

The variation of the shock-layer thickness with the angle θ is shown in figure 13 for the different cases. One effect of body size is an increase in the deviation of the shock-layer thickness for the nonadiabatic cases from that for the adiabatic case. When $r_b = 3$ inches, there is virtually no difference in the shock-layer thickness for the gray and the nongray cases. The nongray shock layers are thicker than the gray ones for the cases with $r_b = 1$ foot and $r_b = 15$ feet. For the case with $r_b = 5$ feet, the gray shock layer has virtually the same thickness as the nongray one in the stagnation region, and it is thicker than the nongray one for larger values of the angle θ.

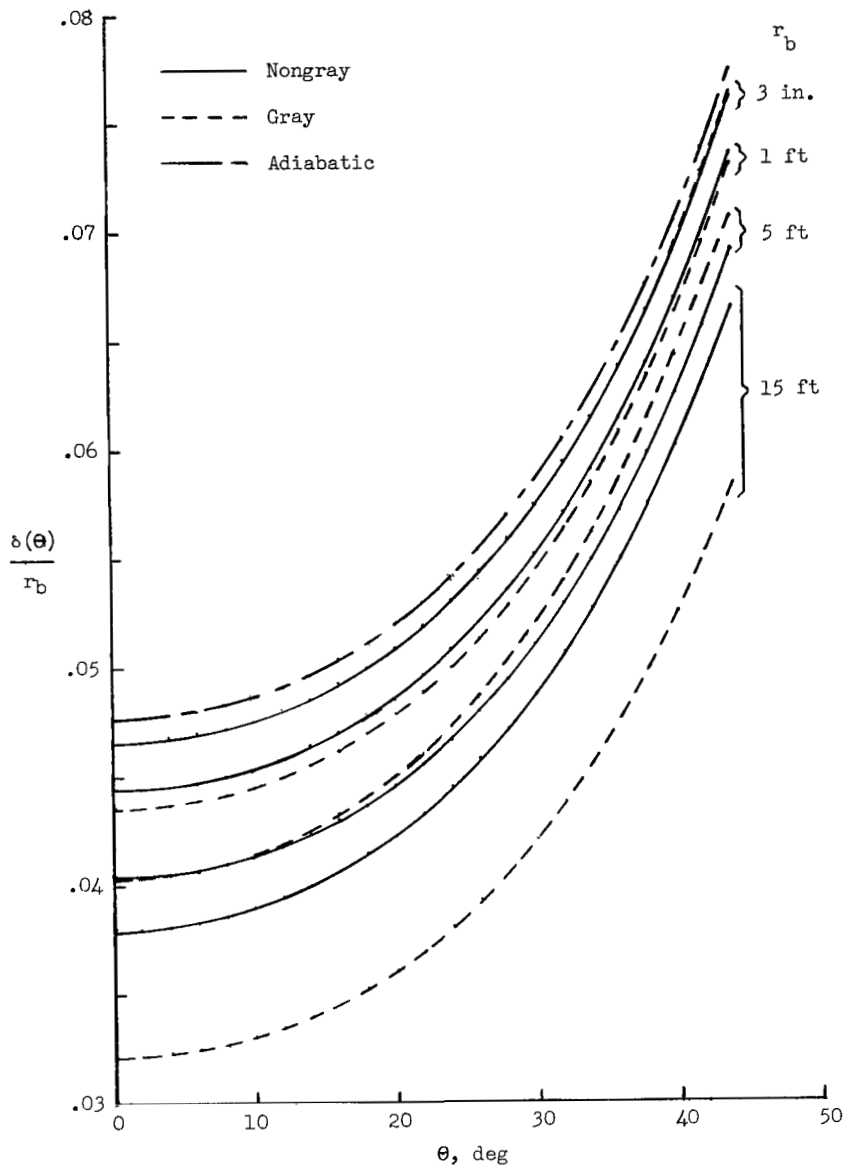

Figure 13.- Effect of size on gray and nongray shock-layer thickness distributions for spheres traveling at 50 000 ft/sec (15.24 km/sec) at an altitude of 190 000 ft (57.91 km).

The shock-detachment distance is governed largely by the rate at which mass is transferred out of the stagnation region. Along the stagnation streamline, this rate is proportional to the product of the density and the tangential velocity gradient. The density is greater for the gray radiation model than for the nongray model at a given point in the stagnation region because the density is inversely proportional to the enthalpy and

the enthalpy for the gray model is less than that for the nongray model, as is shown in figure 12. For the case with $r_b = 5$ feet, the tangential velocity gradient for the nongray model is greater than that for the gray model by an amount which is just enough to compensate for the difference in the density. Therefore, the shock-detachment distances for the two radiation models are the same for $r_b = 5$ feet.

In figure 14, the surface heat-flux distributions for the gray and the nongray radiation models are compared. Values for the stagnation-point heat fluxes are given subsequently. It is seen that differences in the distributions for the two models are small. There is a slight tendency for the differences to increase as the body radius is increased.

The gray and the nongray nondimensional surface heat-flux distributions presented in figure 14 are compared in figures 15(a) and 15(b), respectively, to determine the effect of body size on the distribution shapes. It is seen that this effect is slight for both radiation models. This result is particularly surprising for the nongray model since the relative contributions from the different parts of the spectrum vary considerably as the body radius varies. (See fig. 16.) For the case with $r_b = 3$ inches, the heat flux comes predominantly from that part of the spectrum with $\lambda < 1130$Å. The contributions of the two parts of the spectrum are approximately the same for the case with $r_b = 1$ foot. The heat flux from that portion of the spectrum with $\lambda < 1130$Å is only about 10 percent of the total for the case with $r_b = 5$ feet. For the case with $r_b = 15$ feet, the ultraviolet portion of the spectrum contributes less than 1 percent of the total heat flux. Therefore, a spectral breakdown of this case is not shown in figure 16.

Altitude, 140 000 feet (42.67 km); velocity, 34 000 ft/sec (10.36 km/sec).- Results for spheres traveling in the atmosphere of the earth at an altitude of 140 000 feet (42.67 km) at a velocity of 34 000 ft/sec (10.36 km/sec) are presented in this section. For the flight conditions used in the previous section, the temperature in the hotter portions of the shock layers varies with pressure and density as $p^{.432}/\rho^{.392}$. The hotter portion of the shock layer provides most of the radiant heat which strikes the body surface. Since the heat flux depends strongly on the temperature, it might be expected that different flight conditions would yield different heat-flux distributions. The flight conditions which are used in this section are chosen so that the temperature in the shock layer varies as $p^{.810}/\rho^{.794}$. The nongray surface heat flux is calculated for spheres with radii of 3 inches and 5 feet.

In order to determine the initial solution with equations (E27) and (E29), it is assumed that the temperature varies as $h^{.794}$. Equation (47) is used to obtain the absorption coefficient for the spectral range $1130\text{Å} \leqq \lambda < \infty$ for the cases with $r_b = 3$ inches and 5 feet. For the case with $r_b = 3$ inches, it is assumed that the second

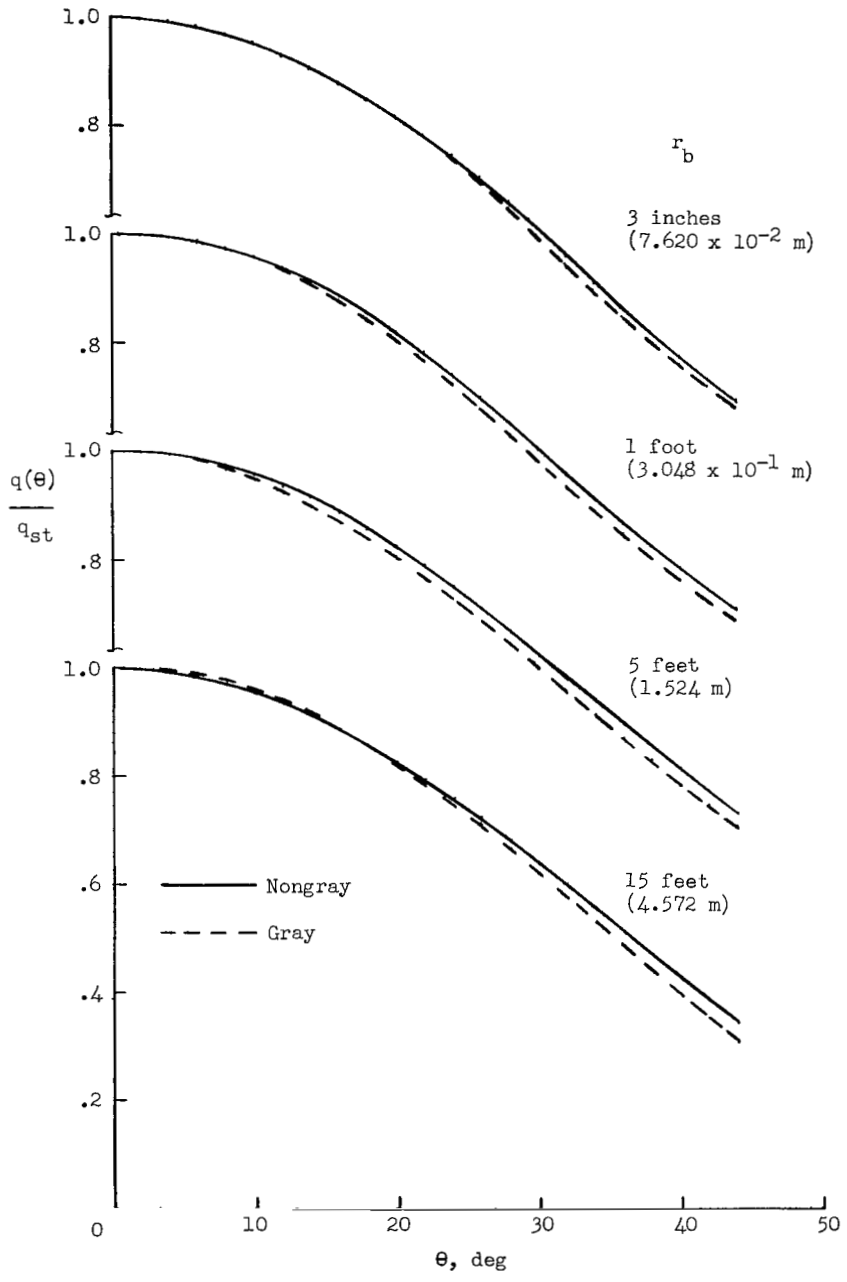

Figure 14.- Gray and nongray surface heat-flux distributions for spheres traveling at 50 000 ft/sec (15.24 km/sec) at an altitude of 190 000 ft (57.91 km).

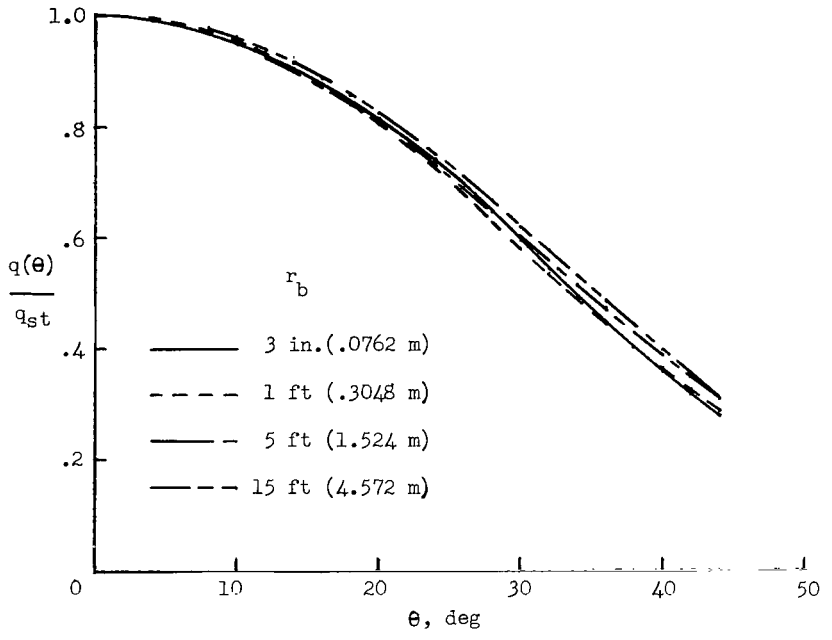

(a) Gray radiation model.

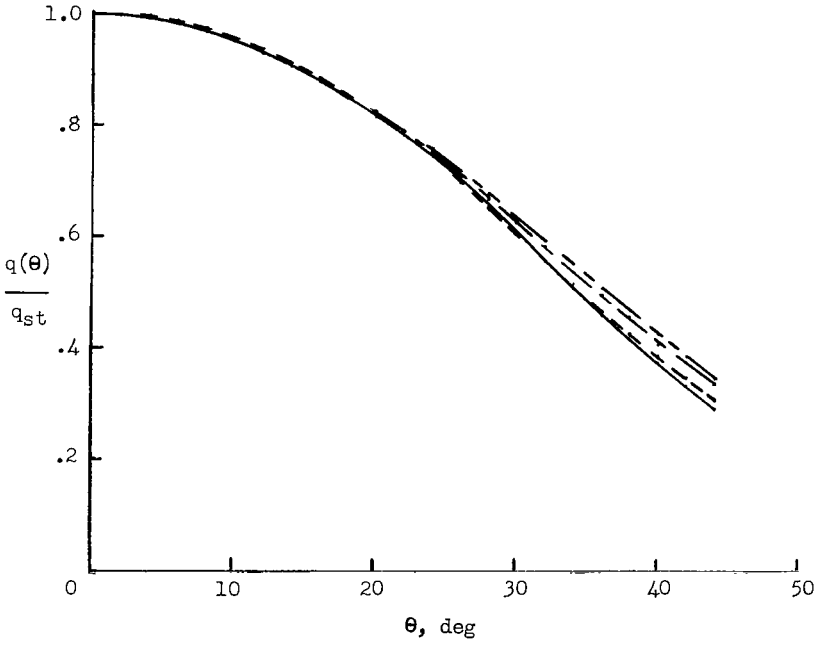

(b) Nongray radiation model.

Figure 15.- Effect of size on the gray and nongray surface heat-flux distributions for spheres traveling at 50 000 ft/sec (15.24 km/sec) at an altitude of 190 000 ft (57.91 km).

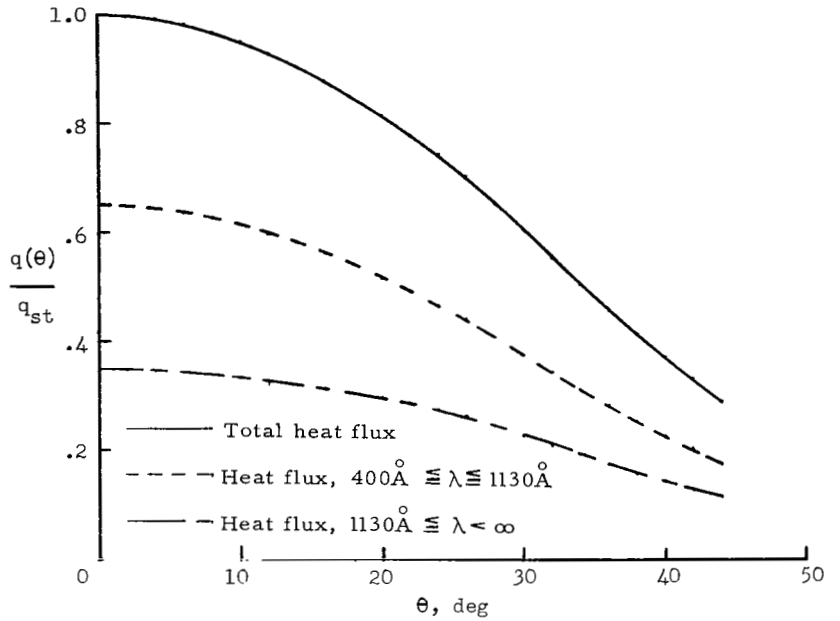

(a) r_b = 3 in. (7.620×10^{-2} m).

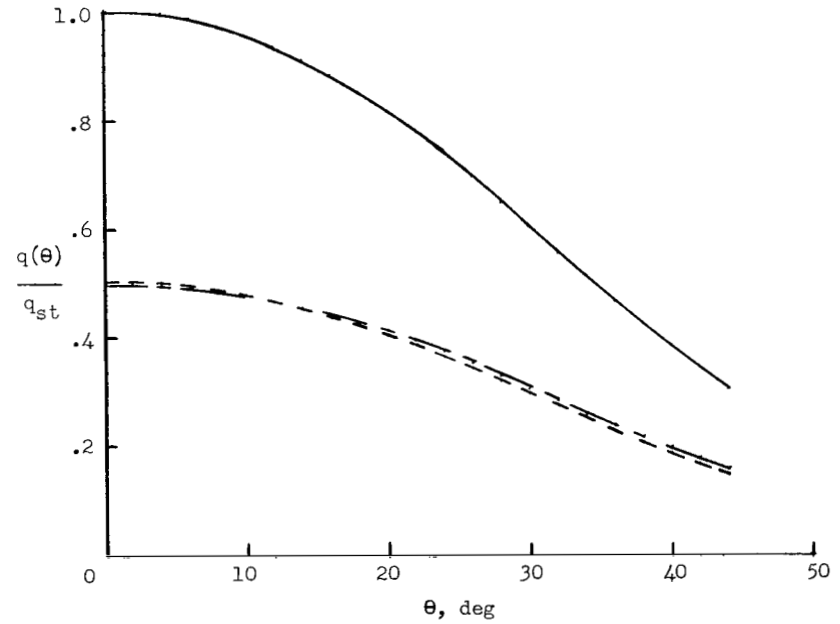

(b) r_b = 1 ft (3.048×10^{-1} m).

Figure 16.- Spectral breakdown of the nongray surface heat-flux distributions for spheres traveling at 50 000 ft/sec (15.24 km/sec) at an altitude of 190 000 ft (57.91 km).

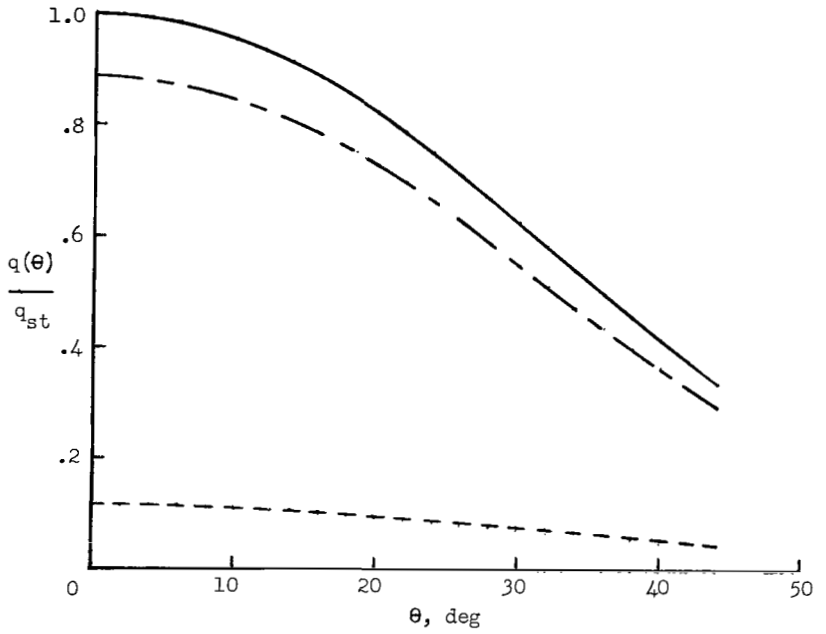

(c) r_b = 5 ft (1.524 m).

Figure 16.- Concluded.

step covers the spectral range $852\text{Å} \leqq \lambda \leqq 1130\text{Å}$. The absorption coefficient for this range is

$$\alpha_2 = 68.15\left(\frac{\rho}{\rho_o}\right)^{1.182}\left(\frac{T}{10^4}\right)^{.329} \text{ cm}^{-1}$$

The radiation for $\lambda < 852\text{Å}$ is optically thick and is neglected. For the case with r_b = 5 feet, the radiation for $\lambda < 1130\text{Å}$ is neglected.

The results for the total nondimensional nongray surface heat-flux distributions for the two cases are shown in figure 17. For the present set of flight conditions, as with the previous set, the distributions are insensitive to body sizes. However, as with the previous flight conditions, the contributions to the heat flux from the portions of the spectrum with $\lambda < 1130\text{Å}$ and $\lambda > 1130\text{Å}$ differ for the two cases. A spectral breakdown for the case with r_b = 3 inches is shown in figure 18. A breakdown for the case with r_b = 5 feet is not given because more than 99 percent of the heat comes from that portion of the spectrum with $\lambda > 1130\text{Å}$.

Effect of flight conditions on surface heat-flux distribution.- The nongray surface heat-flux distributions for the two different sets of flight conditions for spheres with radii

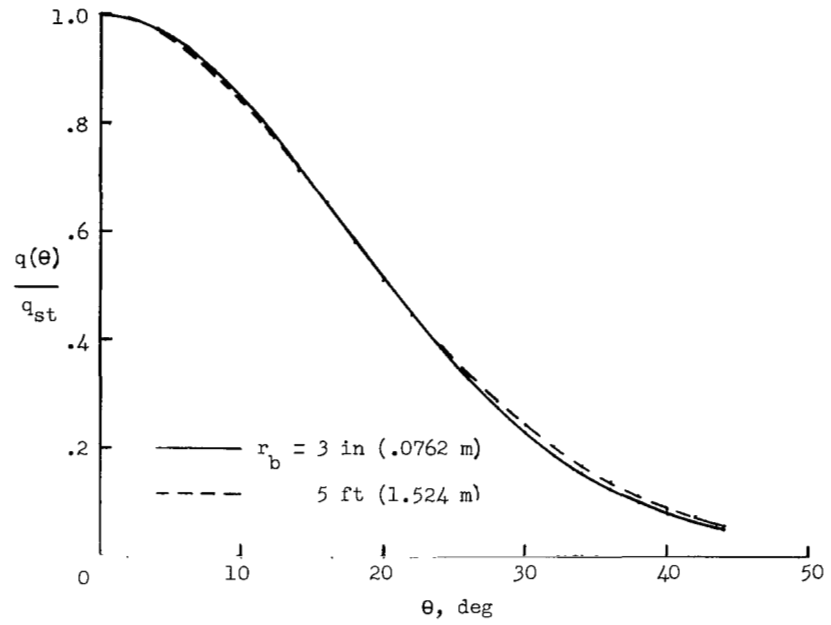

Figure 17.- Effect of size on nongray surface heat-flux distributions for spheres traveling at 34 000 ft/sec (10.36 km/sec) at an altitude of 140 000 ft (42.67 km).

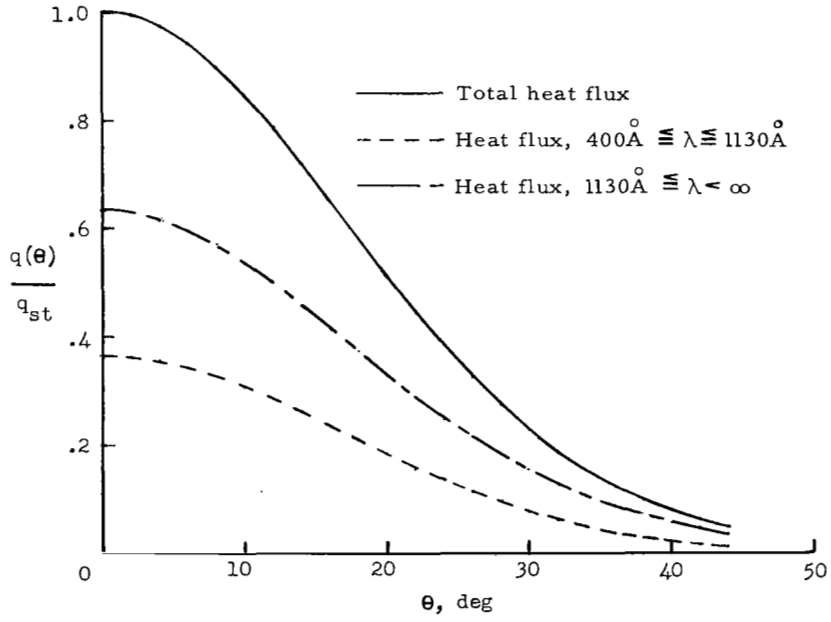

Figure 18.- Spectral breakdown of the nongray surface heat-flux distribution for a sphere with a radius of 3 in. (0.0762 m) traveling at 34 000 ft/sec (10.36 km/sec) at an altitude of 140 000 ft (42.67 km).

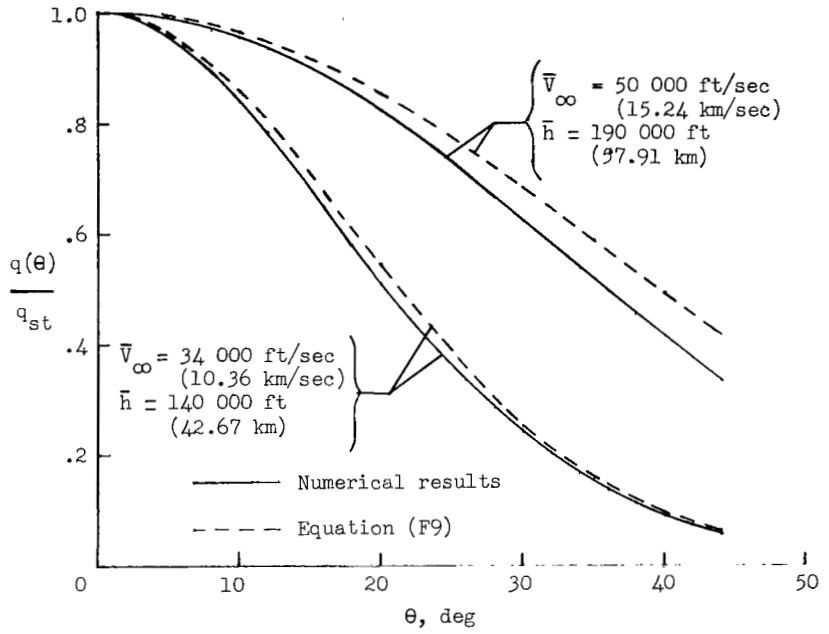

Figure 19.- Approximate analytic solution for nongray surface heat-flux distribution for a sphere with a radius of 5 ft (1.524 m).

of 5 feet are compared in figure 19. Since the variations of the pressure, the density, and the shock-layer thickness with the angle Θ are very nearly the same for the two cases, the difference in the heat-flux distributions must be due to the differences in the dependence of the temperature on the pressure and density and in the dependence of the absorption coefficient on the density and temperature. In order to demonstrate these effects, an approximate analytic solution for the surface heat-flux distribution is developed in appendix F. In figure 19 the approximate results for the nondimensional heating distributions which are determined from equation (F9) show the same trends as the numerical results. The approximate solution accounts only for the radiation from the optically thin portion of the spectrum with $\lambda > 1130$Å since the radiation for $\lambda < 1130$Å is optically thick and is absorbed in the flow field. It should be mentioned that the approximate results for the stagnation-point heat flux which are determined from equation (F10) are greater than those which are determined numerically. This condition occurs because the analytic solution accounts for absorption only in an approximate fashion. For the case with $\bar{V}_\infty = 50\,000$ ft/sec (15.24 km/sec) and $\bar{h} = 190\,000$ ft (57.91 km), equation (F10) yields a value of 0.660 for the nondimensional stagnation-point heat flux $q_{st}/2\alpha_{1,s}\delta(0)\sigma T_s^4$ for $\lambda > 1130$Å. The numerical value for the heat flux for this case is 0.527. For the case with $\bar{V}_\infty = 34\,000$ ft/sec (10.36 km/sec) and $\bar{h} = 140\,000$ ft (42.67 km), the analytic and numerical results for the nondimensional stagnation-point heat flux for $\lambda > 1130$Å are 0.432 and 0.353, respectively.

The exponents $\tilde{a}_1$ and $\tilde{d}$ in equation (F9) are assigned the values 1.2 and 1.3, respectively, for both cases. For the case with $\bar{V}_\infty$ = 50 000 ft/sec (15.24 km/sec) and $\bar{h}$ = 190 000 ft (57.91 km), the exponents $\tilde{b}_1$, $\tilde{R}$, and $\tilde{S}$ and the ratios $\tilde{\gamma}$, $\delta(0)/r_b$, and ρ_{st}/ρ_s have the values 2.3, 0.432, 0.392, 1.129, 0.0404, and 1.87, respectively. The respective values for these parameters for the case with $\bar{V}_\infty$ = 34 000 ft/sec (10.36 km/sec) and $\bar{h}$ = 140 000 ft (42.67 km) are 6.9, 0.810, 0.794, 1.147, 0.051, and 1.29.

Both the altitude and the velocity differ considerably for the two cases which are compared in figure 19. In order to determine the individual effects of altitude and velocity, additional calculations were made for the nongray radiation model and a body with a radius of 5 feet. The results for the total-surface heat-flux distributions for these calculations and those presented in figure 19 are compared in figure 20. For a given flight velocity, the effect of altitude on the surface heat-flux distribution is small. The velocity influences the heat-flux distribution chiefly through the equation of state, which governs the dependence of the temperature on the pressure and density. As stated previously, this dependence is $p^{.432}/\rho^{.392}$ and $p^{.810}/\rho^{.794}$, respectively, for velocities of 50 000 ft/sec (15.24 km/sec) and 34 000 ft/sec (10.36 km/sec). For velocities of 41 000 ft/sec (12.50 km/sec), the dependence of the temperature on the pressure and density varies from approximately $p^{.432}/\rho^{.392}$ on the axis to $p^{.810}/\rho^{.794}$ for large values of the angle Θ.

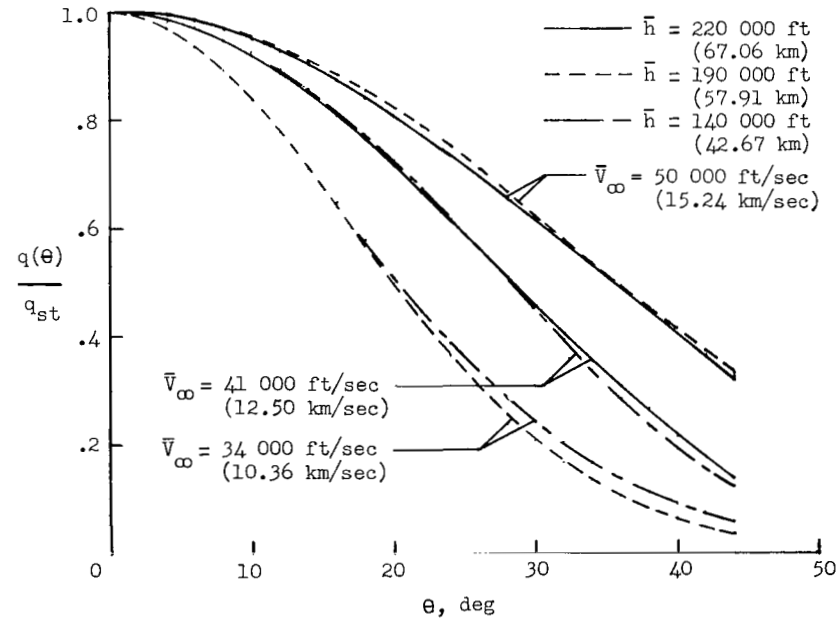

Figure 20.- Effect of flight speed and altitude on nongray surface heat-flux distribution for a sphere with a radius of 5 ft (1.524 m).

Although the shapes of the total nongray heat-flux distributions are very similar for a given flight velocity and different altitudes, the relative contributions from the two portions spectrum to the heat flux vary with altitude. For a velocity of 50 000 ft/sec (15.24 km/sec), the contributions to the heat flux from the optically thin portion of the spectrum with $\lambda > 1130\text{Å}$ are approximately 90 percent and 60 percent, respectively, for altitudes of 190 000 ft (57.91 km) and 220 000 ft (67.06 km). The optically thin portion of the spectrum contributes approximately 100 percent and 65 percent of the surface radiative heat flux for a flight velocity of 41 000 ft/sec and altitudes of 140 000 ft and 220 000 ft. The respective contributions for a velocity of 34 000 ft/sec and altitudes of 140 000 ft and 190 000 ft are approximately 100 percent and 85 percent.

The effect of the shape of the nondimensionalized heat-flux distribution on the total radiative heating to the body can be seen by comparing the ratio of the integral of the heat flux over the surface area with $\Theta \leqq 44^{\circ}$ to the product of this area and the stagnation-point heat flux for the cases shown in figure 20. This ratio, which is written as

$$\frac{\int_{\Theta=0}^{\Theta=44^{\circ}} q(\Theta)\sin\Theta \, d\Theta}{q_{st}\int_{\Theta=0}^{\Theta=44^{\circ}} \sin\Theta \, d\Theta}$$

has values of 0.32, 0.48, and 0.63, respectively, for flight velocities of 34 000 ft/sec, 41 000 ft/sec, and 50 000 ft/sec. These numbers demonstrate that comparisons of stagnation-point heating rates may not yield correct comparisons of the total heating rates for an entry vehicle. This observation has been made for the case of transparent shock layers by several writers. (For example, see ref. 25.)

Stagnation-point heat flux.- The present results for the gray stagnation-point heating rates are compared with those of Thomas (ref. 2) and Olstad (ref. 4) in figure 21. These rates are made nondimensional by dividing by the factor $2\alpha_{P,s}\delta_A\sigma T_s^4$ which is the gray heat flux obtained from an isothermal slab with the thickness of the adiabatic shock layer when absorption is neglected. The quantity against which the rates are plotted is the gray energy depletion parameter Γ, which is defined by equation (46). The results of Thomas and Olstad have been interpolated for a flight velocity of 50 000 ft/sec (15.24 km/sec) and an altitude of 190 000 ft (57.91 km) in the atmosphere of the earth. It is seen that the present results agree more nearly with those of reference 2 than with those of reference 4.

The results for the nongray stagnation-point heating rates are given in table I.

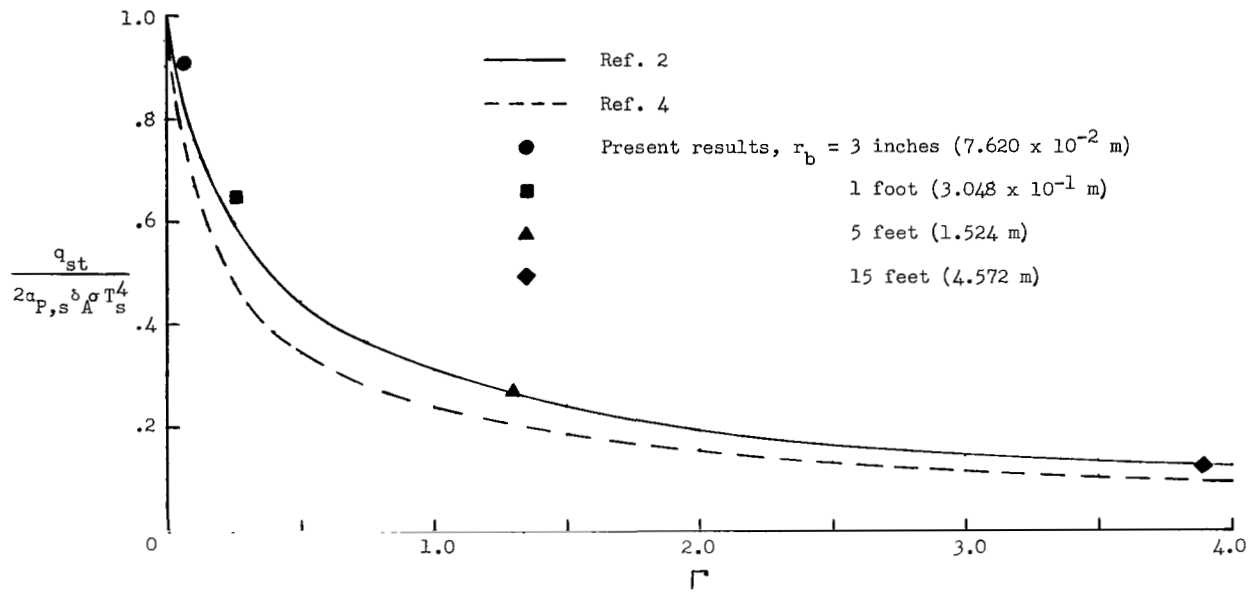

Figure 21.- Gray stagnation-point heat-flux distribution for spheres traveling at 50 000 ft/sec (15.24 km/sec) at an altitude of 190 000 ft (57.91 km).

TABLE I.- NONGRAY STAGNATION-POINT HEAT FLUX

Altitude		Sphere radius		Heat flux	
feet	meters	feet	meters	Btu/ft^2-sec	kW/m^2
Velocity, 50 000 ft/sec (15.24 km/sec)					
190 000	57 910	0.25	0.0762	1 806	20 500
190 000	57 910	1.00	.3048	4 840	54 900
190 000	57 910	5.00	1.524	7 530	85 500
190 000	57 910	15.00	4.572	10 630	120 600
220 000	67 060	5.00	1.524	2 114	24 000
Velocity, 41 000 ft/sec (12.50 km/sec)					
140 000	42 670	5.00	1.524	25 740	292 000
220 000	67 060	5.00	1.524	562	6 380
Velocity, 34 000 ft/sec (10.36 km/sec)					
140 000	42 670	0.25	0.0762	410	4 650
140 000	42 670	5.00	1.524	2 760	31 300
190 000	57 910	5.00	1.524	243	2 760

CONCLUSIONS

On the basis of the results presented, the following conclusions can be stated:

1. Converged solutions for the radiative heat flux which impinges on the surface of an entry vehicle can be obtained with a first-order time-dependent finite-difference method if the grid is refined sufficiently.

2. Only minor differences occur in the results for the nondimensional surface heat-flux distributions for the gray and nongray absorption coefficient models.

3. The shape of the nondimensional heat-flux distributions is a strong function of the flight velocity and a weak function of the size of the body and the altitude.

Langley Research Center,
National Aeronautics and Space Administration,
Langley Station, Hampton, Va., February 19, 1969,
129-01-03-11-23.

APPENDIX A

THE ENERGY EQUATION

Equations (1) to (4) can be combined so that the energy equation can be written as

$$\rho \frac{dh}{dt} - \frac{dp}{dt} = Q$$

If the enthalpy h is replaced by the right-hand side of equation (15) and e is assumed to be a function of p and ρ, this equation becomes

$$\rho\left(\frac{\partial e}{\partial p}\right)_\rho \frac{dp}{dt} + \left[\rho\left(\frac{\partial e}{\partial \rho}\right)_p - \frac{p}{\rho}\right]\frac{d\rho}{dt} = Q \tag{A1}$$

From the first and second laws of thermodynamics,

$$de = \frac{p}{\rho^2} d\rho + T\, dS \tag{A2}$$

where S is the entropy. From equation (A2),

$$\left(\frac{\partial e}{\partial \rho}\right)_S = \frac{p}{\rho^2} \tag{A3}$$

If e is assumed to be of the form $e = e(\rho, p(\rho,S))$, the derivative $(\partial e/\partial \rho)_S$ can be written as

$$\left(\frac{\partial e}{\partial \rho}\right)_S = \left(\frac{\partial e}{\partial \rho}\right)_p + \left(\frac{\partial e}{\partial p}\right)_\rho \left(\frac{\partial p}{\partial \rho}\right)_S \tag{A4}$$

Equating the right-hand sides of equations (A3) and (A4) and noting that

$$\left(\frac{\partial p}{\partial \rho}\right)_S = a^2$$

yields

$$\rho\left(\frac{\partial e}{\partial \rho}\right)_p - \frac{p}{\rho} = -\rho a^2 \left(\frac{\partial e}{\partial p}\right)_\rho \tag{A5}$$

APPENDIX A

By using equation (A5), equation (A1) can be written as

$$\frac{dp}{dt} - a^2 \frac{\partial \rho}{dt} = \frac{Q}{\rho\left(\frac{\partial e}{\partial p}\right)_\rho} \tag{A6}$$

The derivatives $(\partial e/\partial p)_\rho$ and $(\partial e/\partial \rho)_p$ can be determined in terms of ρ, e, and $\tilde{\gamma}(\rho,e)$ by replacing e by the expression

$$e = \frac{1}{\tilde{\gamma}[\rho,e(p,\rho)] - 1}\frac{p}{\rho}$$

and differentiating. The derivative $(\partial e/\partial p)_\rho$ is written as

$$\left(\frac{\partial e}{\partial p}\right)_\rho = \frac{1}{\rho\left[\tilde{\gamma} - 1 + \left(\frac{\partial \tilde{\gamma}}{\partial \log_e e}\right)_\rho\right]} \tag{A7}$$

and the derivative $(\partial e/\partial \rho)_p$ is

$$\left(\frac{\partial e}{\partial \rho}\right)_p = -\frac{e\left[\tilde{\gamma} - 1 + \left(\frac{\partial \tilde{\gamma}}{\partial \log_e \rho}\right)_e\right]}{\rho\left[\tilde{\gamma} - 1 + \left(\frac{\partial \tilde{\gamma}}{\partial \log_e e}\right)_\rho\right]} \tag{A8}$$

With the aid of equation (A7), the energy equation (A6) can be written as

$$\frac{dp}{dt} - a^2 \frac{d\rho}{dt} = \left[\tilde{\gamma} - 1 + \left(\frac{\partial \tilde{\gamma}}{\partial \log_e e}\right)_\rho\right] Q$$

Equations (A5), (A7), and (A8) can be used to write an expression for the square of the speed of sound as

$$a^2 = e\left\{(\tilde{\gamma} - 1)\left[\tilde{\gamma} + \left(\frac{\partial \tilde{\gamma}}{\partial \log_e e}\right)_\rho\right] + \left(\frac{\partial \tilde{\gamma}}{\partial \log_e \rho}\right)_e\right\}$$

APPENDIX B

CURVE FITS FOR THE THERMODYNAMIC FUNCTIONS $\tilde{\gamma}(\rho,e)$ AND $T(p,\rho)$

The data of Allison (ref. 17) and Browne (ref. 18) have been used to construct curve fits for the thermodynamic functions $\tilde{\gamma}(\rho,e) = \frac{h}{e}$ and $T(p,\rho)$.

The function $\tilde{\gamma} = \frac{h}{e}$ for equilibrium air for $10^{-4} \leqq \frac{\rho}{\rho_o} \leqq 10$ and $\frac{e}{RT_o} \leqq 1500$ is given by the following equations:

$$\tilde{\gamma} = 1.405 \qquad \left(\log_{10} \frac{e}{RT_o} \leqq 0.801\right) \tag{B1}$$

$$\tilde{\gamma} = 1.5055 - 0.1255 \log_{10} \frac{e}{RT_o}$$

$$\left(0.801 < \log_{10} \frac{e}{RT_o} \leqq 2.300; \quad \log_{10} \frac{\rho}{\rho_o} \geqq \frac{3.255 - 2.278 \log_{10} \frac{e}{RT_o}}{1 - 0.822 \log_{10} \frac{e}{RT_o}}\right) \tag{B2}$$

$$\tilde{\gamma} = \left(1.6370 - 0.0404 \log_{10} \frac{\rho}{\rho_o}\right) - \left(0.2175 - 0.0332 \log_{10} \frac{\rho}{\rho_o}\right)\log_{10} \frac{e}{RT_o}$$

$$- \frac{\left(0.1366 - 0.0366 \log_{10} \frac{\rho}{\rho_o}\right) - \left(0.0833 - 0.0248 \log_{10} \frac{\rho}{\rho_o}\right)\log_{10} \frac{e}{RT_o}}{1 + \exp\left[-18.30\left(\log_{10} \frac{e}{RT_o} - 1.943 - 0.032 \log_{10} \frac{\rho}{\rho_o}\right)\right]}$$

$$\left(0.801 < \log_{10} \frac{e}{RT_o} \leqq 2.300; \log_{10} \frac{\rho}{\rho_o} < \frac{3.255 - 2.278 \log_{10} \frac{e}{RT_o}}{1 - 0.822 \log_{10} \frac{e}{RT_o}}\right) \tag{B3}$$

$$\tilde{\gamma} = \left(1.5004 - 0.0038 \log_{10} \frac{\rho}{\rho_o}\right) - \left(0.1342 - 0.0084 \log_{10} \frac{\rho}{\rho_o}\right)\log_{10} \frac{e}{RT_o}$$

$$- \frac{\left(0.3274 + 0.0091 \log_{10} \frac{\rho}{\rho_o}\right) - \left(0.1342 + 0.0016 \log_{10} \frac{\rho}{\rho_o}\right)\log_{10} \frac{e}{RT_o}}{1 + \exp\left[-15.85\left(\log_{10} \frac{e}{RT_o} - 2.708 - 0.0320 \log_{10} \frac{\rho}{\rho_o}\right)\right]}$$

$$\left(2.300 < \log_{10} \frac{e}{RT_o} \leqq 3.176\right) \qquad \text{(B4)}$$

The temperature (T in ^{o}K) for equilibrium air for $6.00 \times 10^{-2} \leqq \frac{p}{p_o} \leqq 2.00 \times 10$ and $10^{-3} \leqq \frac{\rho}{\rho_o} \leqq 10^{-1}$ is given by the following equations:

$$\log_{10} T = 4.211 + 0.068R_o - 0.392\left(\log_{10} \frac{\rho}{\rho_o} - R_o\right) - \frac{0.402\left(\log_{10} \frac{\rho}{\rho_o} - R_o\right)}{1 - \exp\left[-50.25\left(\log_{10} \frac{\rho}{\rho_o} - R_o\right)\right]}$$

$$\left(\log_{10} \frac{\rho}{\rho_o} \neq R_o\right) \qquad \text{(B5)}$$

$$\log_{10} T = 4.203 + 0.068 \log_{10} \frac{\rho}{\rho_o} \qquad \left(\log_{10} \frac{\rho}{\rho_o} = R_o\right) \qquad \text{(B6)}$$

where

$$R_o = 0.941 \log_{10} \frac{p}{p_o} - 1.970 \qquad \text{(B7)}$$

APPENDIX C

THE PERFECT GAS MODEL

It is assumed that the ratio $\tilde{\gamma} = \frac{h}{e}$ is constant. By use of this assumption, the energy equation

$$T\,dS = dh - \frac{1}{\rho}\,dp$$

and equations (18) can be combined to obtain

$$\left(\tilde{\gamma} - 1\right) T\,dS = \frac{1}{\rho}\,dp - \tilde{\gamma}\,\frac{p}{\rho^2}\,d\rho \tag{C1}$$

If the equation for the temperature is of the form

$$T = \frac{Cp^{\tilde{R}}}{\rho^{\tilde{S}}}$$

where the exponents $\tilde{R}$ and $\tilde{S}$ are different from one, equation (C1) can be written as

$$\left(\tilde{\gamma} - 1\right) C\,dS = \frac{1}{1 - \tilde{R}}\,\frac{1}{\rho^{1-\tilde{S}}}\,d\left(p^{1-\tilde{R}}\right) + \frac{\tilde{\gamma}}{1 - \tilde{S}}\,p^{1-\tilde{R}}\,d\left(\frac{1}{\rho^{1-\tilde{S}}}\right) \tag{C2}$$

Let subscripts 1, 2, 3, and 4 denote the properties at the points shown in figure 22.

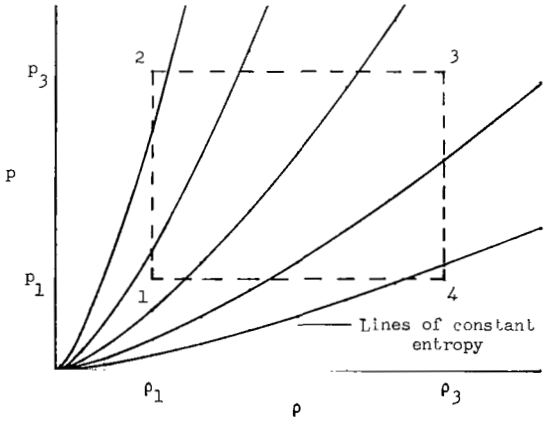

Figure 22.- Schematic of dependence of entropy on pressure and density.

APPENDIX C

When equation (C2) is integrated from the states p_1, ρ_1 to p_3, ρ_3 along the paths 1,2,3 and 1,4,3 as shown in the figure, the following results are obtained:

$$\left(\tilde{\gamma} - 1\right) C\left(S_3 - S_1\right) = \frac{1}{1 - \tilde{R}} \frac{1}{\rho_1^{1-\tilde{S}}}\left(p_2^{1-\tilde{R}} - p_1^{1-\tilde{R}}\right) + \frac{\tilde{\gamma}}{1 - \tilde{S}} p_2^{1-\tilde{R}}\left(\frac{1}{\rho_3^{1-\tilde{S}}} - \frac{1}{\rho_2^{1-\tilde{S}}}\right) \tag{C3a}$$

and

$$\left(\tilde{\gamma} - 1\right) C\left(S_3 - S_1\right) = \frac{\tilde{\gamma}}{1 - \tilde{S}} p_1^{1-\tilde{R}}\left(\frac{1}{\rho_4^{1-\tilde{S}}} - \frac{1}{\rho_1^{1-\tilde{S}}}\right) + \frac{1}{1 - \tilde{R}} \frac{1}{\rho_4^{1-\tilde{S}}}\left(p_3^{1-\tilde{R}} - p_4^{1-\tilde{R}}\right) \tag{C3b}$$

Noting that $\rho_2 = \rho_1$, $p_2 = p_3$, $\rho_4 = \rho_3$, and $p_4 = p_1$, one can equate the right-hand sides of equations (C3) and obtain

$$\left(\frac{p_1^{1-\tilde{R}}}{\rho_1^{1-\tilde{S}}} - \frac{p_2^{1-\tilde{R}}}{\rho_2^{1-\tilde{S}}} + \frac{p_3^{1-\tilde{R}}}{\rho_3^{1-\tilde{S}}} - \frac{p_4^{1-\tilde{R}}}{\rho_4^{1-\tilde{S}}}\right)\left(\frac{1}{1 - \tilde{R}} - \frac{\tilde{\gamma}}{1 - \tilde{S}}\right) = 0 \tag{C4}$$

Since the first factor in equation (C4) does not vanish in general, the following relationship must exist between $\tilde{\gamma}$, $\tilde{R}$, and $\tilde{S}$:

$$1 - \tilde{S} = \tilde{\gamma}\left(1 - \tilde{R}\right)$$

From equation (C1), the expression for the speed of sound for the perfect gas model can be obtained. This equation can be rewritten as

$$dp = \tilde{\gamma} \frac{p}{\rho} d\rho + \left(\tilde{\gamma} - 1\right) \rho T \, dS$$

The equation for the square of the speed of sound is

$$a^2 = \left(\frac{\partial p}{\partial \rho}\right)_s = \frac{\tilde{\gamma} p}{\rho}$$

APPENDIX D

THE RADIATION INTENSITY, HEAT FLUX, AND NET HEAT INPUT PER UNIT VOLUME FOR AN INFINITE, ONE-DIMENSIONAL SLAB OF GAS

Radiation Intensity

The differential equation for the radiation intensity I_ν for a one-dimensional slab is

$$-\frac{\cos\phi}{\alpha_\nu(y)}\frac{\partial I_\nu(y,\phi)}{\partial y} = I_\nu(y,\phi) - B_\nu(y) \tag{D1}$$

where y is the coordinate measured along a line normal to the slab, and ϕ is the angle between the line of propagation of radiation and the y-axis. This coordinate system is shown in figure 23. The y coordinate increases from the body to the shock, and the y coordinates of the body and the shock are y_b and y_s, respectively.

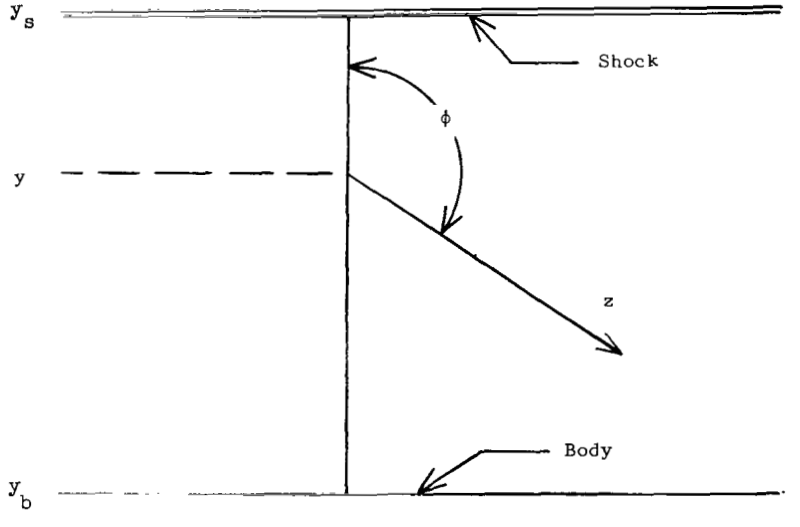

Figure 23.- Geometry of one-dimensional radiating slab.

The integration factors $\exp\left[\sec\phi A_\nu(y_b,y)\right]$ and $\exp\left[\sec(\pi-\phi)A_\nu(y,y_s)\right]$ are used to integrate equation (D1) for $0 \leqq \phi \leqq \pi/2$ and $\pi/2 \leqq \phi \leqq \pi$, respectively, where the integral $A_\nu(r,s)$ is given by equation (40). If it is assumed that the body surface does not reflect, the solution to equation (D1) can be written as

APPENDIX D

$$I_\nu^+(y,\phi) = I_\nu^+(y_b)\exp\left[-\sec\phi A_\nu(y_b,y)\right] + \sec\phi\int_{s=y_b}^{s=y}\alpha_\nu(s)B_\nu(s)\exp\left[-\sec\phi A_\nu(s,y)\right]ds \qquad (0 \leqq \phi \leqq \pi/2) \qquad \text{(D2a)}$$

$$I_\nu^-(y,\phi) = I_\nu^-(y_s)\exp\left[-\sec(\pi-\phi)A_\nu(y,y_s)\right] + \sec(\pi-\phi)\int_{s=y}^{s=y_s}\alpha_\nu(s)B_\nu(s)\exp\left[-\sec(\pi-\phi)A_\nu(y,s)\right]ds \qquad (\pi/2 \leqq \phi \leqq \pi) \qquad \text{(D2b)}$$

where $I_\nu^+(y_b)$ and $I_\nu^-(y_s)$ are the intensities of the radiation entering the slab from the body and the gas in the free stream, respectively.

Heat Flux

In general, the monochromatic heat flux across an elemental area is given by the equation

$$q_\nu = \int_{4\pi} I_\nu \cos\phi \, d\Omega \qquad \text{(D3)}$$

If an infinite slab is being considered, the heat flux across an elemental area which is parallel to the sides of the slab is given by the equation

$$q_\nu(y) = \int_{\psi=0}^{\psi=2\pi}\left[\int_{\phi=0}^{\phi=\pi/2} I_\nu^+(y,\phi)\cos\phi\sin\phi\,d\phi + \int_{\phi=\pi/2}^{\phi=\pi} I_\nu^-(y,\phi)\cos\phi\sin\phi\,d\phi\right]d\psi \qquad \text{(D4)}$$

where ψ is the azimuthal angle. Since I_ν^+ and I_ν^- are independent of the angle ψ, the integration with respect to that variable is straightforward.

It can be seen from equations (D2) that I_ν^+ and I_ν^- are functions of $\sec\phi$ and $\sec(\pi-\phi)$, respectively. When $\sec\phi$ and $\sec(\pi-\phi)$ in the first and second integrals with respect to ϕ in equation (D4), respectively, are replaced by ω, that equation can be written in the form

$$q_\nu(y) = 2\pi\left[\int_{\omega=1}^{\omega=\infty} I_\nu^+(y,\omega)\frac{d\omega}{\omega^3} - \int_{\omega=1}^{\omega=\infty} I_\nu^-(y,\omega)\frac{d\omega}{\omega^3}\right]$$

or

$$q_\nu(y) = 2\pi\left[I_\nu^+(y_b)\int_{\omega=1}^{\omega=\infty} e^{-\omega A_\nu(y_b,y)}\frac{d\omega}{\omega^3} - I_\nu^-(y_s)\int_{\omega=1}^{\omega=\infty} e^{-\omega A_\nu(y,y_s)}\frac{d\omega}{\omega^3}\right.$$

$$+ \int_{s=y_b}^{s=y} \alpha_\nu(s)B_\nu(s)\left(\int_{\omega=1}^{\omega=\infty} e^{-\omega A_\nu(s,y)}\frac{d\omega}{\omega^2}\right)ds$$

$$\left. - \int_{s=y}^{s=y_s} \alpha_\nu(s)B_\nu(s)\left(\int_{\omega=1}^{\omega=\infty} e^{-\omega A_\nu(y,s)}\frac{d\omega}{\omega^2}\right)ds\right] \tag{D5}$$

By using equation (41) to replace the integrals with respect to ω with exponential integrals, equation (D5) can be written as

$$q_\nu(y) = 2\pi\left\{I_\nu^+(y_b)E_3\left[A_\nu(y_b,y)\right] - I_\nu^-(y_s)E_3\left[A_\nu(y,y_s)\right] + \int_{s=y_b}^{s=y} B_\nu(s)E_2\left[A_\nu(s,y)\right]\alpha_\nu(s)ds\right.$$

$$\left. - \int_{s=y}^{s=y_s} B_\nu(s)E_2\left[A_\nu(y,s)\right]\alpha_\nu(s)ds\right\}$$

It can be shown from equations (39) and (40) that

$$\left.\begin{aligned}\frac{dE_n}{ds}\left[A_\nu(s,y)\right] &= E_{n-1}\left[A_\nu(s,y)\right]\alpha_\nu(s)\\ \frac{dE_n}{ds}\left[A_\nu(y,s)\right] &= -E_{n-1}\left[A_\nu(y,s)\right]\alpha_\nu(s)\end{aligned}\right\} \tag{D6}$$

By using equations (D6), the equation for the monochromatic heat flux is

$$q_\nu(y) = 2\pi\left(I_\nu^+(y_b)\ E_3\left[A_\nu(y_b,y)\right] - I_\nu^-(y_s)\ E_3\left[A_\nu(y,y_s)\right]\right.$$

$$\left. + \int_{s=y_b}^{s=y} B_\nu(s)d\left\{E_3\left[A_\nu(s,y)\right]\right\} + \int_{s=y}^{s=y_s} B_\nu(s)d\left\{E_3\left[A_\nu(y,s)\right]\right\}\right) \tag{D7}$$

The total radiative heat flux can be obtained by integrating the monochromatic heat flux over all frequencies:

APPENDIX D

$$q(y) = \int_{\nu=0}^{\nu=\infty} q_\nu(y)d\nu \tag{D8}$$

Net Heat Input to a Volume Element

The net heat input to a volume element due to monochromatic radiation is equal to the negative of the divergence of the monochromatic heat-flux vector $-\vec{\nabla} \cdot \vec{q}_\nu$:

$$Q_\nu = -\vec{\nabla} \cdot \vec{q}_\nu = \alpha_\nu \left(\int_{4\pi} I_\nu \, d\Omega - 4\pi B_\nu \right) \tag{D9}$$

For an infinite slab, $Q_\nu(y)$ is related to $q_\nu(y)$ by the equation

$$Q_\nu(y) = -\frac{dq_\nu(y)}{dy} \tag{D10}$$

The expression which is used in this report to determine the net heat input can be obtained either from the right-hand side of equation (D9) or from equation (D10). The latter equation is used here.

When equation (D7) is integrated by parts, the following expression for $q_\nu(y)$ is obtained:

$$q_\nu(y) = 2\pi \left\{ \left[I_\nu^+(y_b) - B_\nu(y_b) \right] E_3\left[A_\nu(y_b,y)\right] - \left[I_\nu^-(y_s) - B_\nu(y_s) \right] E_3\left[A_\nu(y,y_s)\right] \right.$$
$$\left. - \int_{s=y_b}^{s=y} \frac{dB_\nu(s)}{ds} E_3\left[A_\nu(s,y)\right] ds - \int_{s=y}^{s=y_s} \frac{dB_\nu(s)}{ds} E_3\left[A_\nu(y,s)\right] ds \right\} \tag{D11}$$

From equations (39) and (40), it can be shown that

$$\left.\begin{aligned} \frac{dE_n}{dy}\left[A_\nu(s,y)\right] &= -E_{n-1}\left[A_\nu(s,y)\right]\alpha_\nu(y) \\ \frac{dE_n}{dy}\left[A_\nu(y,s)\right] &= E_{n-1}\left[A_\nu(y,s)\right]\alpha_\nu(y) \end{aligned}\right\} \tag{D12}$$

By using equations (D12) and Leibnitz's rule for differentiating an integral, equation (D11) can be differentiated with respect to y to obtain

APPENDIX D

$$\frac{dq_\nu(y)}{dy} = -2\pi\alpha_\nu(y)\left\{\left[I_\nu^+(y_b) - B_\nu(y_b)\right] E_2\left[A_\nu(y_b,y)\right] + \left[I_\nu^+(y_s) - B_\nu(y_s)\right] E_2\left[A_\nu(y,y_s)\right]\right.$$
$$\left. - \int_{s=y_b}^{s=y} \frac{dB_\nu(s)}{ds} E_2\left[A_\nu(s,y)\right] ds + \int_{s=y}^{s=y_s} \frac{dB_\nu(s)}{ds} E_2\left[A_\nu(y,s)\right] ds\right\} \quad \text{(D13)}$$

By substituting the right-hand side of equation (D13) into equation (D10) and using equations (D6) on the resulting expression, the following expression for the net monochromatic heat input for a volume element in an infinite slab is obtained:

$$Q_\nu(y) = 2\pi\alpha_\nu(y)\left(\left[I_\nu^+(y_b) - B_\nu(y_b)\right] E_2\left[A_\nu(y_b,y)\right] + \left[I_\nu^-(y_s) - B_\nu(y_s)\right] E_2\left[A_\nu(y,y_s)\right]\right.$$
$$\left. - \int_{s=y_b}^{s=y} \frac{1}{\alpha_\nu(s)} \frac{dB_\nu(s)}{ds} d\left\{E_3\left[A_\nu(s,y)\right]\right\} - \int_{s=y}^{s=y_s} \frac{1}{\alpha_\nu(s)} \frac{dB_\nu(s)}{ds} d\left\{E_3\left[A_\nu(y,s)\right]\right\}\right) \quad \text{(D14)}$$

The net heat input due to radiative transfer is obtained by integrating $Q_\nu(y)$ over all frequencies:

$$Q(y) = \int_{\nu=0}^{\nu=\infty} Q_\nu(y) d\nu \quad \text{(D15)}$$

The monochromatic heat flux can be expressed in a form other than equation (D14) by integrating equation (D13) once by parts and substituting the result into equation (D10). The resulting equation is

$$Q_\nu(y) = 2\pi\alpha_\nu(y)\left(I_\nu^+(y_b)\, E_2\left[A_\nu(y_b,y)\right] + I_\nu^-(y_s)\, E_2\left[A_\nu(y,y_s)\right] - 2B_\nu(y)\right.$$
$$\left. + \int_{s=y_b}^{s=y} B_\nu(s)\, d\left\{E_2\left[A_\nu(s,y)\right]\right\} - \int_{s=y}^{s=y_s} B_\nu(s)\, d\left\{E_2\left[A_\nu(y,s)\right]\right\}\right) \quad \text{(D16)}$$

APPENDIX E

STAGNATION STREAMLINE SOLUTION FOR GRAY AND NONGRAY RADIATION MODELS

In this analysis, it is assumed that the pressure is constant along the stagnation streamline. By using this assumption, the energy equation along the stagnation streamline can be written as

$$\rho u \frac{dh}{dy} = \int_{\nu=0}^{\nu=\infty} Q_\nu \, d\nu \tag{E1}$$

where y is the length coordinate measured along the stagnation streamline.

Goulard's stretched coordinate x (ref. 1), which is defined by the differential expression

$$dx = \left(\frac{\rho}{\rho_s}\right)^{1/2} dy \tag{E2}$$

is used in this treatment. As in reference 1, the mass flux normal to the surface is approximated by the equation

$$\rho u = -\frac{\rho_\infty \overline{V}_\infty}{\delta_A} x \tag{E3}$$

where ρ_∞ and $\overline{V}_\infty$ are the density and magnitude of the velocity in the free stream and δ_A is the shock detachment distance for the adiabatic case. Equations (E1), (E2), and (E3) can be combined to yield

$$\frac{-\rho_\infty \overline{V}_\infty}{\delta_A}\left(\frac{\rho}{\rho_s}\right)^{1/2} x \frac{dh}{dx} = \int_{\nu=0}^{\nu=\infty} Q_\nu \, d\nu \tag{E4}$$

It is assumed that the absorption coefficient can be approximated with a step function of the form given in equation (41). Therefore, the divergence of the heat flux is given by the expression:

$$\int_{\nu=0}^{\nu=\infty} Q_\nu \, d\nu = \sum_{N=1}^{M} Q_N \tag{E5}$$

It is further assumed that the first two steps are optically thin and the remainder are optically thick so that

APPENDIX E

$$\alpha_1, \alpha_2 < 1$$

$$\alpha_N > 1 \qquad (N = 3,4, \ldots, M)$$

For the optically thick steps, the expression for the divergence of the heat flux, given by equation (D14) or (D16), is simplified with the Rosselind approximation (ref. 11) to yield

$$Q_N = \frac{4\pi}{3\delta_A} \frac{B_{N,s}}{\left(\alpha_{N,s}\delta_A\right)} \frac{\partial}{\partial \bar{y}} \left[\left(\frac{\alpha_{N,s}}{\alpha_N} \right) \frac{\partial}{\partial \bar{y}} \left(\frac{B_N}{B_{N,s}} \right) \right] \qquad (N = 3,4, \ldots, M) \quad \text{(E6)}$$

where

$$\bar{y} = \frac{y}{\delta_A} \qquad \text{(E7)}$$

and

$$B_N = \int_{\nu=\nu_N}^{\nu=\nu_{N+1}} B_\nu \, d\nu \qquad \text{(E8)}$$

It has been explained previously that the quantities $I_\nu^+(y_b)$ and $I_\nu^-(y_s)$ in equations (D14) and (D16) are assigned values of zero. In order to approximate equation (D16) for the optically thin steps, it is assumed that $B_\nu(s) = B_\nu(y)$ in the integral terms of that equation. The result is written as

$$Q_N = \frac{-2\pi}{\delta_A} \left(\alpha_{N,s}\delta_A\right) B_{N,s} \frac{\alpha_N}{\alpha_{N,s}} \frac{B_N}{B_{N,s}} \left\{ E_2\left[A_N\left(y_b, y\right)\right] + E_2\left[A_N\left(y, y_s\right)\right] \right\} \qquad (N = 1,2)$$

where

$$A_N[r,s] = A_\nu[r,s] \qquad \left(\nu_N \leqq \nu \leqq \nu_{N+1}\right) \quad \text{(E9)}$$

The exponential integrals in this equation are approximated by the simple exponential functions

$$E_2(z) \approx e^{-\sqrt{3}z}$$

The exponential functions, in turn, are approximated by the first two terms of their Taylor expansions. Therefore, the expressions for the divergence of the heat flux for the optically thin steps are written as

APPENDIX E

$$Q_N = \frac{-4\pi}{\delta_A} B_{N,s}\alpha_{N,s}\delta_A \frac{\alpha_N}{\alpha_{N,s}} \frac{B_N}{B_{N,s}}\left[1 - \frac{\sqrt{3}}{2} A_N(y_b,y_s)\right] \qquad (N = 1,2) \quad (E10)$$

Equation (40) is used to obtain the quantity $A_N(y_b,y_s)$ in equations (E10). In this treatment, the contributions to the divergence of the heat flux from the optically thick steps $Q_3, Q_4, \ldots, Q_M$ are neglected. This procedure can be justified if the factors $B_{N,s}/(\alpha_{N,s}\delta_A)$ and $B_{N,s}(\alpha_{N,s}\delta_A)$ in equations (E6) and (E10), respectively, satisfy the following inequalities:

$$B_{1,s}(\alpha_{1,s}\delta_A), B_{2,s}(\alpha_{2,s}\delta_A) >> \frac{B_{N,s}}{(\alpha_{N,s}\delta_A)} \qquad (N = 3,4, \ldots, M)$$

By using equations (E5), (E10), and the preceding assumption, equation (E4) can be written as

$$\rho_\infty \bar{V}_\infty h_s \left(\frac{\rho}{\rho_s}\right)^{1/2} x \frac{d}{dx}\left(\frac{h}{h_s}\right) = 4\pi \sum_{N=1}^{2} B_{N,s}(\alpha_{N,s}\delta_A)\frac{\alpha_N}{\alpha_{N,s}} \frac{B_N}{B_{N,s}}\left[1 - \frac{\sqrt{3}}{2} A_N(y_b,y_s)\right] \quad (E11)$$

In this treatment, it is assumed that $\tilde{\gamma}$ and p are constant along the stagnation streamline. Therefore, it is seen from equations (18) that the density can be expressed in terms of the enthalpy as

$$\frac{\rho}{\rho_s} = \frac{h_s}{h} \qquad (E12)$$

An expression for the temperature in terms of the enthalpy can be obtained by combining equations (37), (E12), and the assumption of constant pressure to yield

$$\frac{T}{T_s} = \left(\frac{h}{h_s}\right)^{\tilde{S}} \qquad (E13)$$

It is assumed that the absorption coefficients can be approximated by power-law expressions of the form

$$\frac{\alpha_N}{\alpha_{N,s}} = \left(\frac{\rho}{\rho_s}\right)^{\tilde{a}_N}\left(\frac{T}{T_s}\right)^{\tilde{b}_N} \qquad (N = 1,2) \quad (E14)$$

Equations (E12), (E13), and (E14) can be combined to yield

APPENDIX E

$$\frac{\alpha_N}{\alpha_{N,s}} = \left(\frac{h}{h_s}\right)^{\tilde{b}_N \tilde{S} - \tilde{a}_N} \tag{E15}$$

It is shown in figure 24 that the function $F\left(\frac{h\nu}{kT}\right)$ given by equation (43) can be approximated by the expression

$$F\left(\frac{h\nu}{kT}\right) = f\left(\frac{h\nu}{kT}\right)^{-\tilde{g}} \tag{E16}$$

for the range $1.15 \geqq \log_{10} \frac{h\nu}{kT} \geqq 0.85$ where $f = 2.42 \times 10^5$ and $\tilde{g} = 7.45$. Equations (E8) and (42) can be used to write B_1 and B_2 as

$$B_1 = \frac{\sigma T^4}{\pi}\left[1 - f\left(\frac{h\nu_2}{kT}\right)^{-\tilde{g}}\right] \approx \frac{\sigma T^4}{\pi} \tag{E17a}$$

$$B_2 = \frac{\sigma T^4}{\pi} f\left[\left(\frac{h\nu_2}{kT}\right)^{-\tilde{g}} - \left(\frac{h\nu_3}{kT}\right)^{-\tilde{g}}\right] = \frac{\sigma T^4}{\pi} \tilde{f}\left(\frac{T}{T_s}\right)^{\tilde{g}} \tag{E17b}$$

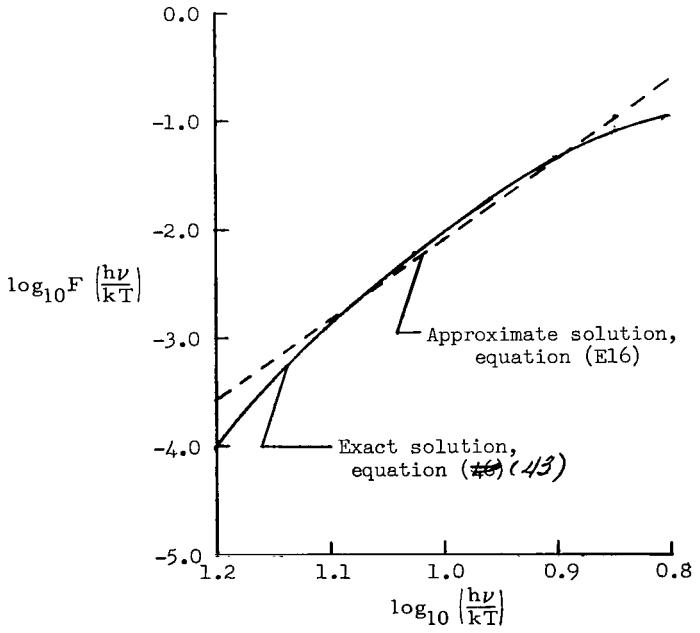

Figure 24.- Approximate solution for integral of Planck function.

where

$$\tilde{f} = f\left[\left(\frac{h\nu_2}{kT_s}\right)^{-\tilde{g}} - \left(\frac{h\nu_3}{kT_s}\right)^{-\tilde{g}}\right] \tag{E18}$$

From equations (E13) and (E17), it follows that

$$\left.\begin{aligned} B_{1,s} &= \frac{\sigma T_s^{\,4}}{\pi} \\ B_{2,s} &= B_{1,s}\tilde{f} \end{aligned}\right\} \tag{E19}$$

and

$$\left.\begin{aligned} \frac{B_1}{B_{1,s}} &= \left(\frac{T}{T_s}\right)^4 = \left(\frac{h}{h_s}\right)^{4\tilde{S}} \\ \frac{B_2}{B_{2,s}} &= \left(\frac{T}{T_s}\right)^{4+\tilde{g}} = \left(\frac{h}{h_s}\right)^{(4+\tilde{g})\tilde{S}} \end{aligned}\right\} \tag{E20}$$

By using equations (E12), (E15), (E19), and (E20), equation (E11) can be written as

$$x\frac{d}{dx}\left(\frac{h}{h_s}\right) = \Gamma_1\left[1 - \frac{\sqrt{3}}{2}A_1\left(y_b,y_s\right)\right]\left(\frac{h}{h_s}\right)^{\left(4+\tilde{b}_1\right)\tilde{S}-\tilde{a}_1+\frac{1}{2}}\left\{1 + \left(\frac{\alpha_{2,s}}{\alpha_{1,s}}\right)\left[\frac{1 - \frac{\sqrt{3}}{2}A_2\left(y_b,y_s\right)}{1 - \frac{\sqrt{3}}{2}A_1\left(y_b,y_s\right)}\right]\tilde{f}\left(\frac{h}{h_s}\right)^{\left(\tilde{b}_2-\tilde{b}_1+\tilde{g}\right)\tilde{S}-\tilde{a}_2+\tilde{a}_1}\right\} \tag{E21}$$

where

$$\Gamma_1 = \frac{4\left(\alpha_{1,s}\delta_A\right)\sigma T_s^{\,4}}{\rho_\infty \overline{V}_\infty h_s} \tag{E22}$$

If a new dependent variable ζ of the form

$$\zeta = \frac{\left(\frac{h}{h_s}\right)^{\tilde{a}_1+\frac{1}{2}-\left(4+\tilde{b}_1\right)\tilde{S}}}{\left[\left(4+\tilde{b}_1\right)\tilde{S} - \tilde{a}_1 - \frac{1}{2}\right]\left[1 - \frac{\sqrt{3}}{2}A_1\left(y_b,y_s\right)\right]\Gamma_1} \tag{E23}$$

is introduced in equation (E21) and the roles of ζ and the independent variable x are reversed, the energy equation can be written as

$$\frac{dx}{d\zeta} + \frac{1}{1 + \frac{\tilde{C}}{\zeta^{\tilde{N}}}}\, x = 0 \tag{E24}$$

where

$$\tilde{N} = \frac{\left(\tilde{b}_2 - \tilde{b}_1 + \tilde{g}\right)\tilde{S} - \tilde{a}_2 + \tilde{a}_1}{\left(4 + \tilde{b}_1\right)\tilde{S} - \tilde{a}_1 - \frac{1}{2}} \tag{E25}$$

and

$$\tilde{C} = \frac{\left(\frac{\alpha_{2,s}}{\alpha_{1,s}}\right)\left[\frac{1 - \frac{\sqrt{3}}{2} A_2\left(y_b, y_s\right)}{1 - \frac{\sqrt{3}}{2} A_1\left(y_b, y_s\right)}\right]^{\tilde{f}}}{\left\{\left[\left(4 + \tilde{b}_1\right)\tilde{S} - \tilde{a}_1 - \frac{1}{2}\right]\left[1 - \frac{\sqrt{3}}{2} A_1\left(y_b, y_s\right)\right]\Gamma_1\right\}^{\tilde{N}}} \tag{E26}$$

Equation (E24) can be integrated by parts to yield

$$x = \delta_A \exp\left\{\frac{1}{\tilde{N} + 1}\left[\frac{\zeta_s}{1 + \frac{\tilde{C}}{\zeta_s^{\tilde{N}}}}\, F\left(1,1;2 + \frac{1}{\tilde{N}};\left[1 + \frac{\tilde{C}}{\zeta_s^{\tilde{N}}}\right]^{-1}\right)\right.\right.$$

$$\left.\left. - \frac{\zeta}{1 + \frac{\tilde{C}}{\zeta^{\tilde{N}}}}\, F\left(1,1;2 + \frac{1}{\tilde{N}};\left[1 + \frac{\tilde{C}}{\zeta^{\tilde{N}}}\right]^{-1}\right)\right]\right\} \tag{E27}$$

where the hypergeometric series is written as

$$F\left(1,1;2 + \frac{1}{\tilde{N}};\left(1 + \frac{\tilde{C}}{\zeta^{\tilde{N}}}\right)^{-1}\right) = 1 + \sum_{i=1}^{\infty} \prod_{j=1}^{i} \left(\frac{j}{j + 1 + \frac{1}{\tilde{N}}}\right)\left(1 + \frac{\tilde{C}}{\zeta^{\tilde{N}}}\right)^{-i} \tag{E28}$$

Two of the parameters in equation (E26) for $\tilde{C}$ are not known initially. These parameters are the optical depths $A_1\left(y_b, y_s\right)$ and $A_2\left(y_b, y_s\right)$. Therefore, the final solution given by equation (E27) must be determined by iteration. Once a preliminary enthalpy

distribution has been obtained, the next approximate values for the optical depths are determined from the equations:

$$A_N(y_b,y_s) = \alpha_{N,s} \int_{\tilde{x}=0}^{\tilde{x}=\delta_A} \left(\frac{h}{h_s}\right)^{\tilde{b}_N\tilde{S}-\tilde{a}_N+\frac{1}{2}} d\tilde{x} \qquad (N = 1,2)$$

The process is repeated until the successive values for the optical depths converge. The final distribution $h(y)$ is determined from the equation

$$y = y_b + \int_{\tilde{x}=0}^{\tilde{x}=x} \left(\frac{h}{h_s}\right)^{1/2} d\tilde{x} \qquad (E29)$$

It can be seen that equation (E27) yields the solution $h = 0$ at the stagnation point $x = 0$. A nontrivial value for the stagnation-point enthalpy is obtained in this treatment by extrapolating the values of the enthalpy h at $x = 0.05\delta_A$ and $x = 0.1\delta_A$.

The results for a gray case and a two-step nongray case are compared with those of Olstad (ref. 4) in figure 25.

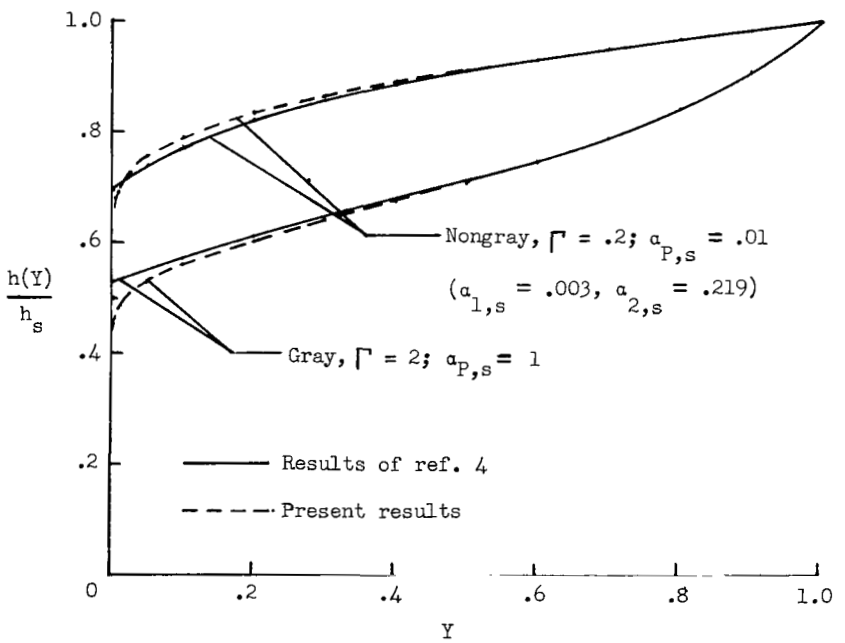

Figure 25.- Comparison of results of present initial solution and those of reference 4 for stagnation-streamline enthalpy distribution.

APPENDIX F

APPROXIMATE SOLUTION FOR SURFACE HEAT FLUX

This solution is derived for shock layers for which most of the radiation which strikes the body surface comes from the optically thin portion of the spectrum with $\lambda > 1130\text{Å}$. Equation (45) for the radiative heat flux to the body surface is approximated by the expression

$$q\left(y_b,\Theta\right) = -2\sigma \int_{s=y_b}^{s=y_s} \alpha_1(s,\Theta)\, T^4(s,\Theta)ds$$

The dependence of the temperature on the pressure and density and the dependence of the absorption coefficient on density and temperature are given by equations (37) and (E14), respectively. Therefore, the equation for the heat flux can be written as

$$q(\Theta) = -2\sigma\alpha_{1,s}\delta(0)\, T_s^4 \frac{\delta(\Theta)}{\delta(0)} \int_{S=0}^{S=1} \frac{\left[\frac{p(\Theta,s)}{p_s}\right]^{\left(4+\tilde{b}_1\right)\tilde{R}}}{\left[\frac{\rho(\Theta,s)}{\rho_s}\right]^{\left(4+\tilde{b}_1\right)\tilde{S}-\tilde{a}_1}} ds \tag{F1}$$

The shock-layer thickness is approximated by the expression

$$\delta(\Theta) = \delta(0)(\cos\Theta)^{-\tilde{d}} \tag{F2}$$

where $\tilde{d}$ is a positive number, and the pressure and density are approximated by expressions linear in Y of the forms

$$\frac{p(Y,\Theta)}{p_s} = Y\cos^2(\Theta - \epsilon) + (1 - Y)\cos^2\Theta \tag{F3}$$

and

$$\frac{\rho(Y,\Theta)}{\rho_s} = Y + \frac{\rho_{st}}{\rho_s}(1 - Y)(\cos\Theta)^{2/\tilde{\gamma}} \tag{F4}$$

The variation of the density along the body surface is determined by assuming that $\tilde{\gamma}$ is constant and that the flow along the surface is isentropic. These conditions are fairly good approximations for the cases treated. Since the angle ϵ in equation (F3) is small, it is assumed that

APPENDIX F

$$\cos \epsilon \approx 1 \tag{F5}$$

Equations (F2) and (22) are used to obtain an approximate expression for $\sin \epsilon$:

$$\sin \epsilon \approx \tan \epsilon = \frac{d\delta/d\Theta}{r_b + \delta} \approx \frac{\tilde{d}\delta(0)\sin \Theta}{r_b + \delta(0)} \tag{F6}$$

By use of equations (F5) and (F6), equation (F3) can be written as

$$\frac{p(Y,\Theta)}{p_s} = \cos^2\Theta + \frac{2\tilde{d}\delta(0)}{r_b + \delta(0)} Y \sin^2\Theta$$

In this treatment, the average value of the pressure across the shock layer is used so that

$$\frac{p(\Theta)}{p_s} = \cos^2\Theta + \frac{\tilde{d}\delta(0)}{r_b + \delta(0)} \sin^2\Theta \approx 1 - \Theta^2 + \frac{\tilde{d}\delta(0)}{r_b + \delta(0)} \Theta^2 \approx (\cos \Theta)^{2\left[1 - \frac{\tilde{d}\delta(0)}{r_b+\delta(0)}\right]} \tag{F7}$$

The integration of the linear expression for the density, which is given by equation (F4), can be performed exactly. The result is written as

$$\int_{s=0}^{s=1} \left[\frac{\rho(\Theta,s)}{\rho_s}\right]^{\tilde{a}_1-\left(4+\tilde{b}_1\right)\tilde{S}} ds = \frac{1 - \left[\frac{\rho_{st}}{\rho_s}(\cos \Theta)^{2/\tilde{\gamma}}\right]^{1+\tilde{a}_1-\left(4+\tilde{b}_1\right)\tilde{S}}}{\left[1 - \frac{\rho_{st}}{\rho_s}(\cos \Theta)^{2/\tilde{\gamma}}\right]\left[1 + \tilde{a}_1 - \left(4 + \tilde{b}_1\right)\tilde{S}\right]} \tag{F8}$$

By using equations (F1), (F2), (F7), and (F8), the approximate expression for the surface heat flux can be written as

$$\frac{q(\Theta)}{q_{st}} = \frac{\left\{1 - \left[\frac{\rho_{st}}{\rho_s}(\cos \Theta)^{2/\tilde{\gamma}}\right]^{1+\tilde{a}_1-\left(4+\tilde{b}_1\right)\tilde{S}}\right\}\left(1 - \frac{\rho_{st}}{\rho_s}\right)(\cos \Theta)^{2\left[1 - \frac{\tilde{d}\delta(0)}{r_b+\delta(0)}\right]\left(4+\tilde{b}_1\right)\tilde{R}-\tilde{d}}}{\left[1 - \left(\frac{\rho_{st}}{\rho_s}\right)^{1+\tilde{a}_1-\left(4+\tilde{b}_1\right)\tilde{S}}\right]\left[1 - \frac{\rho_{st}}{\rho_s}(\cos \Theta)^{2/\tilde{\gamma}}\right]} \tag{F9}$$

The stagnation-point heat flux is given by the expression:

APPENDIX F

$$\frac{q_{st}}{2\alpha_{1,s}\delta(0)\sigma T_s^4} = -\frac{\left[1 - \left(\frac{\rho_{st}}{\rho_s}\right)^{1+\tilde{a}_1-\left(4+\tilde{b}_1\right)\tilde{S}}\right]}{\left(1 - \frac{\rho_{st}}{\rho_s}\right)\left[1 + \tilde{a}_1 - \left(4 + \tilde{b}_1\right)\tilde{S}\right]} \tag{F10}$$

Equation (F9) contains eight parameters. The exponents $\tilde{R}$, $\tilde{S}$, $\tilde{a}_1$, and $\tilde{b}_1$, and the ratio $\tilde{\gamma} = \frac{h}{e}$ can be obtained from thermodynamic and absorption coefficient data. The present results show that the exponent $\tilde{d}$ which governs the variation of the shock-layer thickness with $\cos \Theta$ can be obtained from adiabatic results. The ratios $\frac{\delta(0)}{\left[r_b + \delta(0)\right]}$ and ρ_{st}/ρ_s can be determined from a stagnation streamline treatment. For cases for which the stagnation streamline density profile varies nonlinearly near the body surface, a least-squares procedure should be used to obtain the best linear fit for the density distribution.

The present treatment has not been extended to include the optically thick radiation from the part of the spectrum with $\lambda < 1130\text{Å}$ because most of the radiation in this spectral region which strikes the body surface is emitted close to the surface. This radiation is affected strongly by the density and temperature gradients near the body surface, which are not represented well by this treatment.

REFERENCES

1. Goulard, Robert: Preliminary Estimates of Radiative Transfer Effects on Detached Shock Layers. AIAA J., vol. 2, no. 3, Mar. 1964, pp. 494-502.

2. Thomas, P. D.: Transparency Assumption in Hypersonic Radiative Gasdynamics. AIAA J., vol. 3, no. 8, Aug. 1965, pp. 1401-1407.

3. Howe, John T.; and Viegas, John R.: Solutions of the Ionized Radiating Shock Layer, Including Reabsorption and Foreign Species Effects, and Stagnation Region Heat Transfer. NASA TR R-159, 1963.

4. Olstad, Walter B.: Stagnation-Point Solutions for Inviscid, Radiating Shock Layers. Ph.D. Thesis, Harvard Univ., 1966.

5. Olstad, Walter B.: Blunt-Body Stagnation-Region Flow With Nongray Radiative Heat Transfer – A Singular Perturbation Solution. NASA TR R-295, 1968.

6. Callis, Linwood B.: Time Asymptotic Solutions of Blunt-Body Stagnation-Region Flows With Nongray Emission and Absorption of Radiation. AIAA Paper No. 68-663, June 1968.

7. Wilson, K. H.; and Hoshizaki, H.: Inviscid, Nonadiabatic Flow About Blunt Bodies. AIAA J., vol. 3, no. 1, Jan. 1965, pp. 67-74.

8. Hoshizaki, H.; and Wilson, K. H.: Viscous, Radiating Shock Layer About a Blunt Body. AIAA J., vol. 3, no. 9, Sept. 1965, pp. 1614-1622.

9. Hoshizaki, H.; and Wilson, K. H.: Convective and Radiative Heat Transfer During Superorbital Entry. AIAA J., vol. 5, no. 1, Jan. 1967, pp. 25-35.

10. Cheng, Ping; and Vincenti, Walter G.: Inviscid Radiating Flow Over a Blunt Body. J. Fluid Mech., vol. 27, pt. 4, Mar. 1967, pp. 625-646.

11. Smith, A. M.; and Hassan, H. A.: Nongrey Radiation Effects on the Boundary Layer of an Absorbing Gas Over a Flat Plate. NASA CR-576, 1966.

12. Moretti, Gino; and Abbett, Michael: A Time-Dependent Computational Method for Blunt Body Flows. AIAA J., vol. 4, no. 12, Dec. 1966, pp. 2136-2141.

13. Polachek, Harry: Numerical Analysis. Research Frontiers in Fluid Dynamics, Raymond J. Seeger and G. Temple, eds., Interscience Publ., c.1965, pp. 76-104.

14. Barnwell, Richard W.: Transient Finite Difference Solutions for the Interaction of a Normal Shock Wave With a Sphere and for the Hypersonic Flow of Thermally Radiating Air Past a Sphere. Ph.D. Thesis, Virginia Polytechnic Inst., Sept. 1967.

15. Courant, R.; Friedrichs, K.; and Lewy, H.: Über die partiellen Differenzengleichungen der mathematischen Physik. Math. Ann., vol. 100, 1928, pp. 32-74.

16. Von Mises, Richard: Mathematical Theory of Compressible Flow. Academic Press, Inc., 1958.

17. Allison, Dennis O.: Calculation of Thermodynamic Properties of Gas Mixtures at High Temperatures. M.S. Thesis, Virginia Polytech. Inst., 1965.

18. Browne, W. G.: Thermodynamic Properties of the Earth's Atmosphere. Radiation and Space Phys. Tech. Memo. No. 2, Missile and Space Div., Gen. Elec. Co., Nov. 15, 1962.

19. Grabau, Martin: A Method of Forming Continuous Empirical Equations for the Thermodynamic Properties of Air From Ambient Temperatures to 15,000° K, With Applications. AGARD Rep. 333, Sept. 1959.

20. Hahne, Gerhard E.: The Vacuum Ultraviolet Radiation From N^+- and O^+-Electron Recombination in High-Temperature Air. NASA TN D-2794, 1965.

21. Allen, Richard A.: Air Radiation Graphs: Spectrally Integrated Fluxes Including Line Contributions and Self Absorption. NASA CR-556, 1966.

22. Allen, Richard A.: Air Radiation Tables: Spectral Distribution Functions for Molecular Band Systems. NASA CR-557, 1966.

23. Minzner, R. A.; Champion, K. S. W.; and Pond, H. C.: The ARDC Model Atmosphere, 1959. Air Force Surv. in Geophys. No. 115 (AFCRC-TR-59-267), Air Force Cambridge Res. Center, Aug. 1959.

24. Lomax, Harvard; and Inouye, Mamoru: Numerical Analysis of Flow Properties About Blunt Bodies Moving at Supersonic Speeds in an Equilibrium Gas. NASA TR R-204, 1964.

25. Bobbitt, Percy J.: Effects of Shape on Total Radiative and Convective Heat Inputs at Hyperbolic Entry Speeds. Vol. 13 of Advances in Astronautical Sciences, Eric Burgess, ed., Western Periodicals Co. (N. Hollywood, Calif.), c.1963, pp. 290-319.

"The aeronautical and space activities of the United States shall be conducted so as to contribute . . . to the expansion of human knowledge of phenomena in the atmosphere and space. The Administration shall provide for the widest practicable and appropriate dissemination of information concerning its activities and the results thereof."

—NATIONAL AERONAUTICS AND SPACE ACT OF 1958

NASA SCIENTIFIC AND TECHNICAL PUBLICATIONS

TECHNICAL REPORTS: Scientific and technical information considered important, complete, and a lasting contribution to existing knowledge.

TECHNICAL NOTES: Information less broad in scope but nevertheless of importance as a contribution to existing knowledge.

TECHNICAL MEMORANDUMS: Information receiving limited distribution because of preliminary data, security classification, or other reasons.

CONTRACTOR REPORTS: Scientific and technical information generated under a NASA contract or grant and considered an important contribution to existing knowledge.

TECHNICAL TRANSLATIONS: Information published in a foreign language considered to merit NASA distribution in English.

SPECIAL PUBLICATIONS: Information derived from or of value to NASA activities. Publications include conference proceedings, monographs, data compilations, handbooks, sourcebooks, and special bibliographies.

TECHNOLOGY UTILIZATION PUBLICATIONS: Information on technology used by NASA that may be of particular interest in commercial and other non-aerospace applications. Publications include Tech Briefs, Technology Utilization Reports and Notes, and Technology Surveys.

Details on the availability of these publications may be obtained from:

SCIENTIFIC AND TECHNICAL INFORMATION DIVISION

NATIONAL AERONAUTICS AND SPACE ADMINISTRATION

Washington, D.C. 20546